J|A|C|S
ARTICLES
Published on Web 04/07/2006

Intermolecular Transfer of Copper Ions from the CopC Protein of *Pseudomonas syringae*. Crystal Structures of Fully Loaded $Cu^{I}Cu^{II}$ Forms

Lianyi Zhang,[†] Melissa Koay,[†] Megan J. Maher,*[,‡,§] Zhiguang Xiao,*[,†] and Anthony G. Wedd[†]

Contribution from the School of Chemistry and Bio21 Institute, University of Melbourne, Parkville, VIC 3010, Australia, and School of Molecular and Microbial Biosciences, University of Sydney, Sydney, NSW 2006, Australia

Received January 9, 2006; E-mail: z.xiao@unimelb.edu.au; m.maher@imperial.ac.uk

Abstract: CopC is a small soluble protein expressed in the periplasm of *Pseudomonas syringae* pathovar *tomato* as part of its copper resistance response (cop operon). Equilibrium competition reactions confirmed two separated binding sites with high affinities for Cu^{I} ($10^{-7} \geq K_D \geq 10^{-13}$ M) and Cu^{II} ($K_D = 10^{-13(1)}$ M), respectively. While Cu^{I}-CopC was converted cleanly by O_2 to Cu^{II}-CopC, the fully loaded form $Cu^{I}Cu^{II}$-CopC was stable in air. Variant forms H1F and H91F exhibited a lower affinity for Cu^{II} than does the wild-type protein while variant E27G exhibited a higher affinity. Cation exchange chromatography detected each of the four different types of intermolecular copper transfer reactions possible between wild type and variant forms: Cu^{I} site to Cu^{II} site; Cu^{II} site to Cu^{I} site; Cu^{I} site to Cu^{I} site; Cu^{II} site to Cu^{II} site. The availability of an unoccupied site of higher affinity induced intermolecular transfer of either Cu^{I} or Cu^{II} in the presence of O_2 while buffering concentrations of cupric ion at sub-picomolar levels. Crystal structures of two crystal forms of wild-type $Cu^{I}Cu^{II}$-CopC and of the *apo*-H91F variant demonstrate that the core structures of the molecules in the three crystal forms are conserved. However, the conformations of the amino terminus (a Cu^{II} ligand) and the two copper-binding loops (at each end of the molecule) differ significantly, providing the structural lability needed to allow transfer of copper between partners, with or without change of oxidation state. CopC has the potential to interact directly with each of the four cop proteins coexpressed to the periplasm.

Introduction

Copper is an essential element whose accessible oxidation states Cu^{I} and Cu^{II} form an efficient redox couple when bound at enzyme active sites. However, the same couple can generate toxic oxygen radicals when copper ions are "free" in solution. Consequently, copper levels are tightly controlled in the yeast cytosol (and presumably in other organisms) by specific binding of copper ions to chaperone, pump, and enzyme molecules.[1,2] Both copper uptake and efflux (resistance) pathways work dynamically to maintain appropriate nutritional levels.

The bacterium *Escherichia coli* carries a number of chromosomal operons which mediate copper tolerance.[3] However, copper resistance (the ability to survive elevated environmental levels) requires plasmid-based resistance genes and the *E. coli pco* cluster, for example, features the seven genes *pcoABCDRSE*.[4−6] On the other hand, copper resistance in *Pseudomonas syringae* pathovar *tomato*, a strain isolated from plants treated with copper-based antimicrobial and antifungal agents, carries six plasmid-born genes *copABCDRS* which are homologous to the equivalent *pco* genes.[7,8] They confer some spectacular properties. Cells turn blue upon exposure to high concentrations of copper. The metal accumulates in the periplasmic space, and up to 12% of the dry weight of the cells is copper. An operational model for expression and control is presented in Scheme 1.[6,7,9,10] CopA and CopC are soluble proteins present in the oxidizing environment of the periplasm, CopB and CopD appear to be membrane-bound copper pumps while CopS and CopR form part of copper sensing and gene induction systems.

The CopC protein is proposed to be a copper carrier (Scheme 1),[7,11] but in contrast to known cytoplasmic copper chaperones,

[†] University of Melbourne.
[‡] University of Sydney.
[§] Current address: Division of Molecular Biosciences, Imperial College, London, SW7 2AZ, UK.

(1) Rae, T. D.; Schmidt, P. J.; Pufahl, R. A.; Culotta, V. C.; O'Halloran, T. V. *Science (Washington, D.C.)* **1999**, *284*, 805−808.
(2) Finney, L. A.; O'Halloran, T. V. *Science (Washington, D.C.)* **2003**, *300*, 931−936.
(3) Huffman, D. L.; O'Halloran, T. V. *Annu. Rev. Biochem.* **2001**, *70*, 677−701.
(4) Tetaz, T. J.; Luke, R. K. J. *J. Bacteriol.* **1983**, *154*, 1263−1268.
(5) Brown, N. L.; Barrett, S. R.; Camakaris, J.; Lee, B. T. O.; Rouch, D. A. *Mol. Microbiol.* **1995**, *17*, 1153−1166.
(6) Lee, S. M.; Grass, G.; Rensing, C.; Barrett, S. R.; Yates, C. J. D.; Stoyanov, J. V.; Brown, N. L. *Biochem. Biophys. Res. Commun.* **2002**, *295*, 616−620.
(7) Cooksey, D. A. *FEMS Microbiol. Rev.* **1994**, *14*, 381−386.
(8) Silver, S.; Phung, L. T. *Annu. Rev. Microbiol.* **1996**, *50*, 753−789.
(9) Puig, S.; Rees, E. M.; Thiele, D. J. *Structure (Cambridge, MA)* **2002**, *10*, 1292−1295.
(10) Huffman, D. L.; Huyett, J.; Outten, F. W.; Doan, P. E.; Finney, L. A.; Hoffman, B. M.; O'Halloran, T. V. *Biochemistry* **2002**, *41*, 10046−10055.

10.1021/ja058528x CCC: $33.50

Scheme 1. Partial Model for Copper Resistance in *P. syringae* (cop) and *E. coli* (pco)[a]

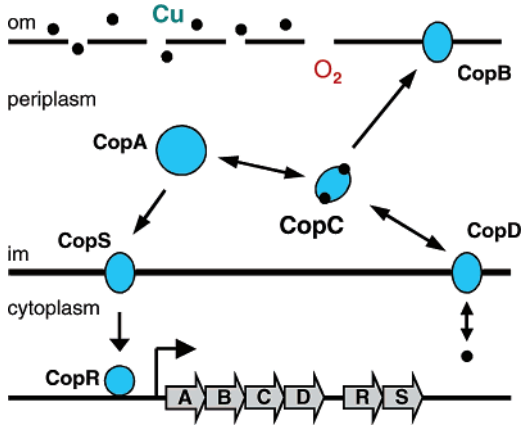

[a] om, outer membrane; im, inner membrane.

it contains no cysteine residues (e.g., see refs 2, 12). NMR and EXAFS structural data revealed a β-barrel topology and two copper binding sites, separated by ~30 Å (Figure 1).[13,14] One site is specific for Cu^{I} while the second is specific for Cu^{II}. The suggested ligand environments are $Cu^{I}(His)(Met)_x$ ($x = 2$ or 3) and $Cu^{II}(His)_2(Asp)(Glu)(OH_2)$. Three of a total of four His residues are proposed as ligands (H48 for Cu^{I}; H1, H91 for Cu^{II}) as are at least two of the four Met residues M40, M43, M46, and M51 (Figure 2). Complementary EXAFS information is available for the homologous *E. coli* protein PcoC with ENDOR and ESEEM spectroscopies consistent with the presence of a tetragonal Cu^{II} site with three nitrogen ligand atoms and one aqua ligand.[10,15] Crystal structures of *apo*-PcoC (wild-type and Se-Met forms) reveal that the β-barrel molecules form weakly associated dimers in the solid state.[16] The four Met residues in the region of the proposed Cu^{I} site of each molecule form part of interacting hydrophobic surfaces.

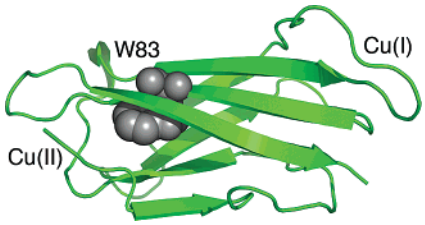

Figure 1. Ribbon representation of the averaged molecular structure of CopC. The relative positions of the Cu^{I} and Cu^{II} sites are shown. Residue W83 is highlighted.

While Cys-rich sites are characteristic of copper(I) carriers in the reducing cytoplasm,[3,17] His/Met-rich sites seem to be important in oxidizing environments. As well as the *cop* and *pco* systems discussed above, such sites are present in the prokaryotic *cue* and *cus* systems, in the bacterial chaperone DR1885 and the eukaryotic Ctr membrane-bound pumps.[18−23] A $Cu^{I}NS_2$ site of trigonal planar geometry has recently been characterized structurally in the $Cu^{I}(His)(Met)_2$ center of CusF.[20]

The present work explores the fundamental chemistry of CopC. It confirms the presence of two separate but interdependent binding sites, one with high specific affinity for Cu^{I} and the other for Cu^{II}. The structural lability of the two sites is revealed for the fully loaded $Cu^{I}Cu^{II}$ form in crystals obtained at both pH 7.5 and 4.5. If the Cu^{I} site only is occupied in solution, the Cu^{+} ion is oxidized rapidly by dioxygen. However, if the Cu^{II} site is also occupied, the Cu^{I} site is stable. The availability of an unoccupied site of higher affinity in wild-type or variant forms induces intermolecular transfer of *either* Cu^{I} or Cu^{II} while buffering free cupric ion concentrations at sub-picomolar levels. This unique copper chemistry is consistent with a role for CopC as a Cu carrier in the oxidizing periplasm (Scheme 1). Some preliminary aspects of this work have been communicated.[24]

Materials and Methods

Characterization and manipulations of CopC and its variants could be carried out aerobically except for certain Cu^{I} forms (wild type, H91F). These were generated anaerobically in deoxygenated buffers and solvents in sealed containers in a glovebox ($[O_2] < 2$ ppm). The samples were kept sealed during transfer from the glovebox for characterization.

Plasmids and Site Directed Mutagenesis. The pAT2 plasmid for CopC expression was a kind gift from Dr. A. R. Thompsett (CERM, University of Florence). Mutagenesis of CopC gene was carried out by PCR targeting the intended mutation site(s) with overlapping primers carrying the designed variation(s). Each variant generated was confirmed by DNA sequencing.

Protein Expression and Purification. Apo-CopC protein was expressed and isolated essentially as reported[13] with an extra gel-filtration purification step. Negatively charged *E. coli* proteins were removed by passing the lysate supernatant through a DE anion exchange column in 20 mM tris-Cl buffer at pH 8. The flow-through fraction was adjusted to pH 6 with 0.2 M mes and then applied to a CM cation exchange column in 20 mM mes at pH 6. The bound proteins were eluted with a salt gradient of 0−0.3 M NaCl in 20 mM mes. Edta (1 mM) was included in the CM buffer to ensure removal of possible contaminating metal ions. *apo*-CopC protein eluted over the range 0.10−0.15 M NaCl. Figure S1 documents the purification via SDS-PAGE. The final purification step used a Superdex-75 gel-filtration column (120 mL, 1.6 cm) with eluent 20 mM KPi, pH 7 and 100 mM NaCl to remove edta and also a minor component of higher molar mass (<2%). Protein yields varied between 50 and 100 mg per L of culture. The identity of the wild type and each variant protein was confirmed by ESI-MS (Table S1; Figure S2). The metal content was <0.01 equiv of copper.

Concentration Assays. Stock solutions of Cu(II) in milli-Q water were standardized via titration with bcs in the presence of hydroxyl-

(11) Cha, J. S.; Cooksey, D. A. *Proc. Natl. Acad. Sci. U.S.A.* **1991**, *88*, 8915−8919.
(12) Urvoas, A.; Moutiez, M.; Estienne, C.; Couprie, J.; Mintz, E.; Le Clainche, L. *Eur. J. Biochem.* **2004**, *271*, 993−1003.
(13) Arnesano, F.; Banci, L.; Bertini, I.; Thompsett, A. R. *Structure (Cambridge, MA)* **2002**, *10*, 1337−1347.
(14) Arnesano, F.; Banci, L.; Bertini, I.; Mangani, S.; Thompsett, A. R. *Proc. Natl. Acad. Sci. U.S.A.* **2003**, *100*, 3814−3819.
(15) Peariso, K.; Huffman, D. L.; Penner-Hahn, J. E.; O'Halloran, T. V. *J. Am. Chem. Soc.* **2003**, *125*, 342−343.
(16) Wernimont, A. K.; Huffman, D. L.; Finney, L. A.; Demeler, B.; O'Halloran, T. V.; Rosenzweig, A. C. *JBIC, J. Biol. Inorg. Chem.* **2003**, *8*, 185−194.
(17) Tottey, S.; Harvie, D. R.; Robinson, N. J. *Acc. Chem. Res.* **2005**, *38*, 775−783.
(18) Outten, F. W.; Outten, C. E.; Hale, J.; O'Halloran, T. V. *J. Biol. Chem.* **2000**, *275*, 31024−31029.
(19) Roberts, S. A.; Weichsel, A.; Grass, G.; Thakali, K.; Hazzard, J. T.; Tollin, G.; Rensing, C.; Montfort, W. R. *Proc. Natl. Acad. Sci. U.S.A.* **2002**, *99*, 2766−2771.
(20) Loftin, I. R.; Franke, S.; Roberts, S. A.; Weichsel, A.; Heroux, A.; Montfort, W. R.; Rensing, C.; McEvoy, M. M. *Biochemistry* **2005**, *44*, 10533−10540.
(21) Banci, L.; Bertini, I.; Ciofi-Baffoni, S.; Katsari, E.; Katsaros, N.; Kubicek, K.; Mangani, S. *Proc. Natl. Acad. Sci. U.S.A.* **2005**, *102*, 3994−3999.
(22) Dancis, A.; Yuan, D. S.; Moehle, C.; Askwith, C.; Eide, D.; Moehie, C.; Kaplan, J.; Klausner, R. D. *Cell (Cambridge, MA)* **1994**, *76*, 393−402.
(23) Puig, S.; Lee, J.; Lau, M.; Thiele, D. J. *J. Biol. Chem.* **2002**, *277*, 26021−26030.
(24) Koay, M.; Zhang, L.; Yang, B.; Maher, M. J.; Xiao, Z.; Wedd, A. G. *Inorg. Chem.* **2005**, *44*, 5203−5205.

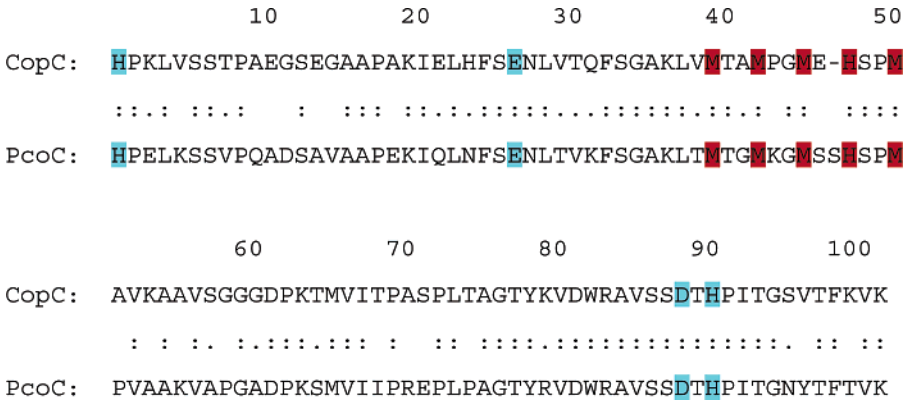

Figure 2. Comparison of amino acid sequence in the plasmid-based copper resistance homologues CopC (*P. syringae*; accession no. aaa25808) and PcoC (*E. coli*; accession no. s52255). Possible ligands for the Cu^{I} and Cu^{II} sites of CopC are in red and teal, respectively.[13]

Table 1. Molar Absorptivities (ϵ, M^{-1} cm^{-1}) at 280 nm of CopC Proteins

apo, □□	$Hg^{II}Hg^{II}$,[a]	$Hg^{II}Cu^{II}$,[a]	□Cu^{II}	$Cu^{I}Cu^{II}$	Cu^{I}X
8700	17 500	19 000	10 600	11 100	9200

[a] Determined at protein concentrations of 150 μM ($Hg^{II}Hg^{II}$) and 120 μM ($Hg^{II}Cu^{II}$) (see Figure 11).

amine.[25] A calibration curve was constructed using solutions obtained by diluting either a commercial standard ($CuSO_4$, 1.575 mM; Aldrich) or one prepared by dissolving the pure salt $[Cu^{I}(MeCN)_4]ClO_4$ quantitatively in de-oxygenated MeCN.

The concentrations of edta and egta used for estimation of dissociation constants were calibrated with a Cu^{II} standard in the presence of a Cu^{II} colorimetric reagent diacetylbis(N4-methyl-3-thiosemicarbazone) (atsm).[26] Briefly, a Cu^{II} standard (1.00 mM) was titrated, with constant stirring, into a 30% dmso solution (2.0 mL) containing edta or egta (ca. 100 μM) and atsm (ca. 50 μM) while absorbance at 457 nm (characteristic of the orange complex Cu^{II}(atsm)) was monitored. With efficient stirring to avoid local excess concentrations of Cu^{2+}, the added Cu^{2+} ions bound preferentially to edta or egta. Cu^{II}(edta) did not exchange metal with atsm while Cu^{II}(egta) exchanged slowly ($t_{1/2}$ ~2 h) with the exchange equilibrium favoring Cu^{II} binding to egta at pH 8.5. A linear increase in absorbance at 457 nm signaled saturation of edta or egta with Cu^{2+}. A plot of A_{457} versus added Cu^{2+} provided a reliable estimation of edta and egta concentrations from the intercept where $A_{457} = 0$.

Protein concentrations were estimated from the absorbance at 280 nm. A calculation based on the protein amino acid content estimated $\epsilon_{280} = 6970$ M^{-1} cm^{-1}. However, titration of *apo*-CopC with standardized Cu^{II} solution monitored by solution absorbance and fluorescence spectra (see Figures 4, 10) estimated a value of 8700 M^{-1} cm^{-1}, on the assumption that CopC binds a single equivalent of Cu^{II}. This value permitted estimation of ϵ_{280} values for a number of metalated species via titration with standardized solutions of the metal ions (Table 1). The values in Table 1 for the various copper forms were confirmed independently by analysis of copper content for each pure protein sample isolated (e.g., see Table 2). The same values were assumed for equivalent forms of the variant proteins.

Generation and Analysis of Metalated Forms. The *apo*-CopC protein and its variants were metalated by addition of Cu^{II} and/or Cu^{I}, followed by gel filtration or cation exchange chromatography to remove weakly bound copper ions. Copper content in each isolated protein sample was determined spectrophotometrically by reaction with at least 20 equiv (relative to protein) of Cu(I)-specific colorimetric reagent bathocuproine disulfonate (bcs).[25] Cu^{I} content was determined directly without addition of reductant. Total copper content (and hence Cu^{II} content by difference) was estimated by subsequent addition of the reductant NH_2OH to the same solution. Typical results form part of Table 2.

Table 2. Analytical Data for Each Protein Component Eluted from the Mono-S Cation Exchange Column (Figures 13, 15, 16, S3)[a]

entry	figure	concn NaCl[b] (mM)	molar mass[c] (Da)	Cu^{I}:CopC	Cu^{II}:CopC	assignment
1	13a; 16b	~40	10 533	nd[d]	nd	wt[e] □□
2	13b, g	~63	10 533	1.0	1.0	wt $Cu^{I}Cu^{II}$
3	13c, f; 16a	~48	10 533	<0.06	1.0	wt □Cu^{II}
4	13d, f, g	0−30[b]	10 542	nd	nd	H1F □X
5	13e	~53	10 542	1.0	nd	H1F Cu^{I}X
6	15a, b, c	~6	10 542	nd	nd	H91F □↓
7	15a	~54	10 542	<0.05	0.9	H91F □Cu^{II}
8	15b	~68	10 542	present[f]	present[f]	H91F $Cu^{I}Cu^{II}$,[f]
9	15c	~77	10 542	present	present	H91F $Cu^{I}Cu^{II}$,[f]
10	15d	~72	10 542	0.9	0.9	H91F $Cu^{I}Cu^{II}$
11	S3		10 542	1.0	1.0	H91F $Cu^{I}Cu^{II}$
12	16a	~112	10 461	1.0	1.0	E27G $Cu^{I}Cu^{II}$
13	16b	~93	10 461	< 0.06	1.0	E27G □Cu^{II}

[a] Protein concentrations were estimated by A_{280} using ϵ_{280} values listed in Table 1; Cu^{I} and Cu^{II} concentrations were estimated spectrophotometrically by reagent bcs as detailed in Materials and Methods.[25] [b] Observed elution concentrations depended on protein concentration, ionic strength, and sample volume so some variation was observed from experiment to experiment. The *apo*-H1F protein □X showed little affinity for Mono-S resin at pH 7, eluting as a broad band of variable position close to the start of the NaCl gradient. [c] Determined as *apo*-form by ESI-MS in acidic solvent. [d] Not detected. [e] Wild type. [f] Both Cu^{I} and Cu^{II} were detected qualitatively but not quantitatively due to the low relative yields. However, their elution positions match that of an authentic $Cu^{I}Cu^{II}$-H91F sample isolated from a gel-filtration column (Figures 15d, S3, Table 2, entries 10,11).

Analytical Methods. Cation Exchange Chromatography. Effective separation of *apo*-CopC and various metalated forms was achieved via NaCl gradient elution on a Mono-S cation exchange column (HR5/5; Pharmacia) in KPi (10 mM; pH 7). The identity of each eluted protein component was established by ESI-MS analysis under acidic conditions while its Cu^{I} and Cu^{II} content were estimated by copper analysis (see Table 2).

Gel Filtration Chromatography. Both the *apo* and metalated forms of CopC were analyzed via elution on a Superdex-75 gel filtration column (HR10/30; Pharmacia) at a flow rate of 0.6 mL/min in KPi buffer (25 mM; pH 7) and NaCl (100 mM) (Figure S3). The column was calibrated with Blue Dextran (2000 kDa), albumin (67 kDa), ovalbumin (43 kDa), chymotrypsinogen A (25 kDa), and ribonuclease A (13.7 kDa) as standards (Amersham Pharmacia).

Physical Measurements. Absorption spectroscopy was performed on a Varian Cary 50 spectrophotometer in dual beam mode with quartz cuvettes of 0.5 or 1 cm path length. Steady-state fluorescence spectra were obtained on a Varian Cary Eclipse spectrophotometer. For

(25) Blair, D.; Diehl, H. *Talanta* **1961**, *7*, 163−174.
(26) Xiao, Z.; Donnelly, P.; Wedd, A. G. Unpublished observations.

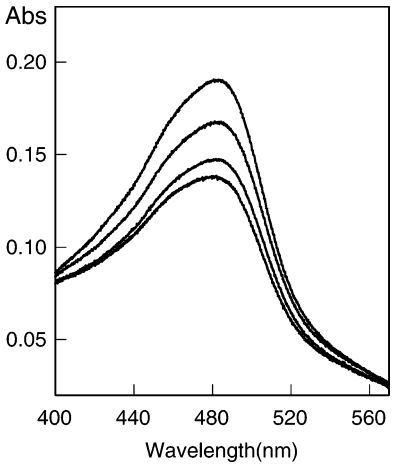

Figure 3. Decrease in intensity of the absorption spectrum of $[Cu^{I}(bcs)_2]^{3-}$ (Cu^{I}, 15 μM; bcs, 45 μM) with increasing concentration of wild type *apo*-CopC □□ in mes buffer (20 mM; pH 6; NaCl, 100 mM) under anaerobic conditions. From top: $[\square\square]_t$ = 0, 250, 500, 750 μM, respectively.

fluorescence emission spectra, the excitation wavelength was 280 nm with a band-pass of 10 nm for both excitation and emission spectra. The spectra were recorded between 295 and 500 nm at a scan rate of 600 nm/min. The absorbance of protein solutions was maintained below A_{280} = 0.1 to minimize resorption effects.

ESI mass spectra were recorded on a Micromass Quattro II Triple-Quadrupole mass spectrometer in the positive ion mode with a cone voltage set at 25−35 V and a flow rate at 30 μL min^{-1}. Protein samples were desalted aerobically with water and diluted to ca. 20 pmol/μL. The diluted samples were mixed with an equal volume of methanol containing 0.1% formic acid just before delivery to the electrospray probe. The average molar masses were obtained by applying a deconvolution algorithm to the recorded spectra and were calibrated with horse heart myoglobin (16 951.5 Da).

Sedimentation equilibrium experiments were carried out at 20 °C using a Beckman Optima XL-A analytical ultracentrifuge with an An-Ti60 rotor. Samples (60 μM) were prepared in potassium phosphate or sodium acetate buffers (50 mM; KPi, pH 6.8; NaAc, pH 4.5) and NaCl (100 mM) by buffer exchange from concentrated protein stocks. Protein solutions and reference buffers were loaded into the ultracentrifuge cells and sedimentation equilibrium distributions determined from radial scans at 280 nm. The final equilibrium distributions were fitted globally using the program SEDEQ1B (kindly provided by Allen Minton, NIH, Bethesda, MD). The partial specific volume of the protein (0.741 g/mL) was calculated from the amino acid composition.

Estimation of Metal Dissociation Constants. The imperatives for optimal estimation of metal ion−protein affinities have been reviewed recently.[27] An approach developed previously for estimation of affinity of proteins for Cu^{I} was adapted and is based on the following competition with ligand bathocupröine disulfonate (bcs):[28]

$$\textit{apo}\text{-CopC} + [Cu^{I}(bcs)_2]^{3-} \Leftrightarrow Cu^{I}\text{-CopC} + 2\ bcs^{2-} \qquad (1)$$

Since CopC binds to Cu^{I} much more weakly than does bcs, the following conditions were necessary to induce competition: (i) to lower the initial bcs/Cu^{I} ratio to 3 (a minimum value to ensure that all Cu^{I} not bound to the protein was present as $[Cu^{I}(bcs)_2]^{3-}$ of known stability constant, $\beta_2 = 10^{19.8}$ M^{-2}); (ii) to add a large molar excess of *apo*-CopC into the solution. Competition was evident from a stepwise decrease in absorbance at 483 nm (characteristic of $[Cu^{I}(bcs)_2]^{3-}$) upon stepwise increase in total CopC concentration under anaerobic conditions (Figure 3; Table S2). The derived $K_D(Cu^{I})$ was 10^{-13} M and must be considered to be a minimum value as these experiments are at the detection limit: <1% of protein molecules bind Cu^{I} at equilibrium. Within experimental error, $K_D(Cu^{I})$ was the same for the variant proteins H1F- and H91F-CopC whose Cu^{I} forms are more stable in air (see below).

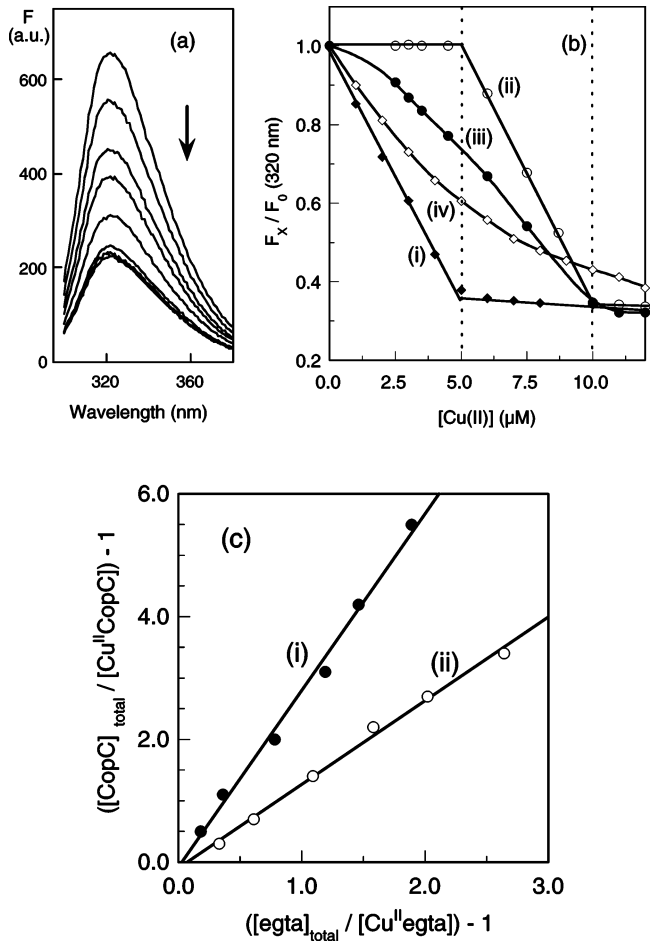

Figure 4. Determination of Cu^{II} dissociation constants $K_D(\square Cu^{II})$ for CopC proteins (5 μM) in KPi buffer (20 mM; pH 7.0; NaCl,100 mM). (a) Quenching of fluorescence emission intensity for *apo*-CopC □□ upon titration with Cu^{2+} solution (200 μM); (b) Change in fluorescence emission intensity as a function of Cu^{II} concentration in the presence of (i) □□ in KPi buffer only; (ii) □□ and edta (5.0 μM); (iii) □□ and egta (5.0 μM); (iv) *apo*-H1F (□X) in KPi buffer only; (c) Plots of eq 3 (Table 6) for effective competition for Cu^{II} between egta and (i) □□; (ii) *apo*-E27G (□↑).

The affinity of CopC proteins for Cu^{II} was estimated by competition with ligands ethyleneglycol-*O*,*O*′-bis(2-aminoethyl)-*N*,*N*,*N*′,*N*′-tetraacetic acid (egta) and *N*,*N*,*N*′,*N*′-ethylenediamine tetraacetic acid (edta). *apo*-CopC fluoresced intensely at λ_{max} 320 nm when excited at 280 nm (Figure 4a). Titration of *apo*-CopC with Cu^{II} quenched the fluorescence intensity linearly until 1 equiv of Cu^{II} was bound (Figure 4a, 4b(i)). If 1 equiv of edta was also present in the *apo*-CopC solution, linear quenching occurred only in the range 1−2 equiv of Cu^{II} (Figure 4b(ii)). Conversely, titration of edta into Cu^{II}CopC led to complete restoration of the fluorescence intensity. The results demonstrated that, under the conditions, *apo*-CopC has a significantly lower affinity for Cu^{II} than does edta (K_A, 3.2 × 10^{15} M^{-1}; pH 7.0; *I*, 100 mM).[29] They also demonstrate that neither edta nor Cu^{II}(edta) perturb the fluorescence intensities of *apo*-CopC or Cu^{II}CopC.

The equivalent experiments with ligand egta produced the titration curve of Figure 4b(iii), demonstrating effective competition for Cu^{II}

(27) Magyar, J. S.; Godwin, H. A. *Anal. Biochem.* **2003**, *320*, 39−54.

(28) Xiao, Z.; Loughlin, F.; George, G. N.; Howlett, G. J.; Wedd, A. G. *J. Am. Chem. Soc.* **2004**, *126*, 3081−3090.

(29) Martell, A. E., Smith, R. M., Eds. *Critical Stability Constants, Vol. 1: Amino Acids*; Plenum: New York, 1974.

between *apo*-CopC and egta (eq 2):

$$\textit{apo}\text{-CopC} + \mathrm{Cu^{II}(egta)} \leftrightarrow \mathrm{Cu^{II}}\text{-CopC} + \mathrm{egta} \quad (2)$$

Within experimental error, the same titration curve (Figure 4b(iii)) was constructed from individual titration experiments that initiated reaction 2 from either direction. These observations permitted reliable estimation of $K_D(Cu^{II})$ for CopC. The following relationship can be derived for effective competition via eq 2 (see Supporting Information for details):

$$K_D K_A = \{([\mathrm{CopC}]_{total}/[\mathrm{Cu^{II}}\text{-CopC}]) - 1\}/\{([\mathrm{egta}]_{total}/[\mathrm{Cu^{II}(egta)}]) - 1\} \quad (3)$$

where K_D is the dissociation constant of Cu^{II}-CopC and K_A is the apparent association constant of Cu^{II}(egta) under the experimental conditions. At pH 7.0 and *I*, 0.1 M, $K_A(Cu^{II}egta)$ is calculated to be 4.0×10^{13} M^{-1}.[29] A plot of $\{([P]_{total}/[CuP]) - 1\}$ versus $\{([egta]_{total}/[Cu^{II}(egta)]) - 1\}$ should generate a straight line with a slope equal to K_DK_A passing through the origin, allowing estimation of K_D.

As in our previous approach,[28] the experiments were carried out in both directions of eq 2 with Cu(II) preloaded on either egta or CopC. Briefly, for forward reactions, a series of individual solutions were generated by adding varying proportions of standardized Cu^{2+} solution to a defined molar quantity of standardized egta solution, followed by addition of equimolar *apo*-CopC. For the reverse reaction, a set of the same solutions was generated but the order of addition of egta and *apo*-CopC was reversed. The mixtures were diluted with KPi buffer (20 mM; pH 7.0; NaCl, 100 mM) so that the final concentrations of both egta and CopC were 5.0 μM. After incubation overnight, the fluorescence spectrum of each solution was recorded and the change in fluorescence intensity (ΔF_X) relative to *apo*-CopC (F_0) was calculated. Equilibration of eq 2 was signaled by the observation of experimentally identical ΔF_X values for each pair of equivalent solutions. Since Cu^{II} binding to CopC quenched the fluorescence intensity linearly until 1 equiv of Cu^{II} was bound, the denominator of eq 3 could be calculated: $[\mathrm{CopC}]_{total}/[\mathrm{Cu^{II}CopC}] = \Delta F_1/\Delta F_X$, where ΔF_1 and ΔF_X are the changes in fluorescence intensity when CopC is loaded with 1 and *x* equiv of Cu^{II}. Mass balance considerations under Cu^{II} limiting conditions then allowed the denominator to be estimated. Results for wild-type CopC and the E27G variant are displayed in Figure 4c.

CopC affinity for Hg^{II} was estimated directly from the change in solution spectrum upon titration of Hg^{2+} into either *apo*-CopC or Cu^{II}-CopC of different concentrations.

X-ray Crystallography of CopC Proteins. Crystal Growth and Analysis. Crystallization conditions were screened for the Cu^ICu^{II} forms of the wild-type and H91F proteins at 293 K according to the sparse-matrix method[30] using commercially available screens (Crystal Screen, Crystal Screen 2, and Salt Rx screen, Hampton Research, Laguna Hills, CA) and the hanging-drop vapor-diffusion technique. For wild-type proteins, small crystals were observed in condition 40 of the Salt Rx screen (6.0 M ammonium nitrate, 0.1 M sodium acetate, pH 4.6). Further refinement of the crystallization conditions produced crystals of typical dimensions $90 \times 90 \times 70$ μm^3 which were grown at room temperature by mixing the protein solution (1.0 μL, 14 mg/mL) with an equal volume of reservoir solution (4.4−5.2 M ammonium nitrate, 0.1 M sodium acetate, pH 4.6−4.8; low pH form). An additional crystal (high pH form) of dimensions $400 \times 400 \times 300$ μm^3 was observed in Crystal Screen condition 39 (2.0 M ammonium sulfate, 0.1 M sodium HEPES, pH 7.5, 2% (w/v) PEG 400). Crystallization experiments with the Cu^ICu^{II} forms of the H91F protein produced crystals in condition 2 of the Salt Rx screen (2.8 M sodium acetate, pH 7.0, 0.1 M Bis-Tris propane, pH 7.0). Further refinement of the crystallization conditions produced crystals of typical dimensions $150 \times 150 \times 150$ μm^3, which were grown at room temperature by mixing protein solution (2.0 μL, 30 mg/mL) with an equal volume of reservoir solution (2.4 M sodium acetate, pH 7.0, 0.1 M Bis-Tris propane, pH 6.6) and edta (0.5 μL, 0.1 M).

Crystals of the wild-type protein were transferred directly into a cold N_2 gas stream (100 K) for data collection following brief (10 s) immersion in the appropriate cryoprotectant solution (low pH form: 6.0 M ammonium nitrate, 0.1 M sodium acetate, pH 4.6, 21% (w/v) xylitol; high pH form: 2.2 M ammonium sulfate, 2% (w/v) PEG 400, 0.1 M sodium Hepes, pH 7.5, 30% (v/v) glycerol). A single crystal of the H91F form was mounted at room temperature using the MicroRT system (MiTeGen, Ithaca, NY). A small amount of reservoir solution was injected at one end of a thin-walled polyester tubing which had been presealed at the other end. The tubing was pulled down over the crystal, which had been mounted on a MicroMount (MiTeGen) and sealed onto the goniometer base with a small amount of vacuum grease. Data from a single crystal of the low pH form were collected at the Stanford Synchrotron Radiation Laboratory on a BL9-2 at a single energy (8999.57 eV), corresponding to the peak position of the Cu K-edge. Subsequent native data sets for the low and high pH forms, in addition to diffraction data from a crystal of the H91F protein, were recorded on an Mar345 image-plate detector with Cu Kα X-rays from a Rigaku RU-200 rotating anode generator focused using Osmic mirror optics. All data were processed and scaled with the *HKL* suite of programs, *DENZO*, and *SCALEPACK*.[31] Statistics for the data collections are presented in Table 3a and b.

Structure Solution and Refinement. Data collected from the low pH form at SSRL were used to solve the structure by single wavelength anomalous dispersion phasing (SAD). The positions of six copper atoms were found and refined, and phases were calculated using SOLVE.[32] Solvent flattening and initial model tracing were carried out by RESOLVE.[33,34] At this point, by interpreting the phased electron density map, the NMR model of *apo*-CopC (PDB coordinates 1M42)[13] could be positioned into the asymmetric unit at three positions. Manual fitting of the model was carried out by the program O.[35] Refinement proceeded using Refmac5,[36] with tight noncrystallographic symmetry (NCS) restraints. NCS restraints were relaxed and finally removed as the refinement progressed.

A single CopC molecule from the structure of the low pH form, with copper atoms and water molecules removed, was used as the search model to find the position and orientation of one molecule of CopC within the asymmetric unit of the high pH form. The molecular replacement was carried out with PHASER and the refinement with Refmac5.[37,38]

The refined structure of the high pH form (with Cu atoms, water molecules, and residue His 91 removed) was used to find the position and orientation of a single molecule of H91F-CopC within the asymmetric unit. The molecular replacement calculation was carried out using MolRep.[39] After initial rounds of refinement using Refmac5,[40] the site of the H91F variation was clearly visible in difference Fourier electron density maps. This variation was incorporated into the model,

(30) Jancarik, J.; Kim, S. H. *J. Appl. Crystallogr.* **1991**, *24*, 409−411.
(31) Otwinowski, Z.; Minor, W. *Methods Enzymol.* **1997**, *276*, 307−326.
(32) Terwilliger, T. C.; Berendzen, J. *Acta Crystallogr., Sect. D: Biol. Crystallogr.* **1999**, *D55*, 849−861.
(33) Terwilliger, T. C. *Acta Crystallog., Sect. D: Biol. Crystallogr.* **2000**, *D56*, 965−972.
(34) Terwilliger, T. C. *Acta Crystallogr., Sect. D: Biol. Crystallogr.* **2003**, *D59*, 38−44.
(35) Jones, T. A.; Zou, J. Y.; Cowan, S. W.; Kjeldgaard, M. *Acta Crystallogr., Sect. A: Found. Crystallogr.* **1991**, *47 (Pt 2)*, 110−119.
(36) Murshudov, G. N.; Vagin, A. A.; Dodson, E. J. *Acta Crystallogr., Sect. D: Biol. Crystallogr.* **1997**, *D53*, 240−255.
(37) Storoni, L. C.; McCoy, A. J.; Read, R. J. *Acta Crystallogr., Sect. D: Biol. Crystallogr.* **2004**, *D60*, 432−438.
(38) Read, R. J. *Acta Crystallogr., Sect. D: Biol. Crystallogr.* **2001**, *D57*, 1373−1382.
(39) Vagin, A.; Teplyakov, A. *J. Appl. Crystallogr.* **1997**, *30*, 1022−1025.

Table 3. Crystallographic Data and Refinement Statistics for (a) $Cu^{I}Cu^{II}$-CopC Proteins and (b) the *apo*-H91F Protein[a]

(a) $Cu^{I}Cu^{II}$-CopC Proteins

	low pH form		high pH form
crystallization pH	4.6−4.8	4.6−4.8	7.5
radiation source	SSRL	rot. anode	rot. anode
X-ray wavelength (Å)	1.3776	1.5418	1.5418
space group	$P3_221$	$P3_221$	$P4_32_12$
unit cell parameters			
a (Å)	104.9	104.5	55.8
c (Å)	56.0	55.5	60.3
mosaicity (deg)	0.52	0.79	1.16
resolution (Å)	50.0−2.8 (2.9−2.8)	50.0−2.25 (2.33−2.25)	50.0−1.6 (1.66−1.60)
unique observations	16 908	16 159	13 027
total observations	85 608	79 068	171 605
completeness (%)	99.9 (98.9)	96.1 (97.4)	99.6 (100.0)
redundancy	5.1 (3.3)	4.9 (4.7)	13.2 (11.0)
$I/\sigma(I)$	12.2 (3.6)	13.7 (3.1)	33.0 (7.9)
R_{merge}[b]	0.112 (0.366)	0.076 (0.388)	0.067 (0.324)

Refinement Statistics

	low pH form	high pH form
no. molecules/asu	3	1
resolution range (Å)	50.0−2.25	40.0−1.6
no. protein residues	306	102
no. of Cu atoms	6	2 (1 with occupancy 0.75)
no. of water molecules	205	83
no. of other entities	4 (NO_3^-)	0
total no. of atoms	2461	860
reflections	16 151	12 982
R_{cryst}[c]	0.190 (0.252)	0.187 (0.221)
R_{free}[c,d]	0.263 (0.360)	0.225 (0.292)
rms Δ − bond lengths (Å)	0.005	0.012
rms Δ − bond angles (deg)	0.952	1.538
average protein *B*-value (Å^2)	41.7	24.6
ESU (Å)[e]	0.18	0.06
Ramachandran plot, residues in: [f]		
most favored regions (%)	97.6	93.9
additional allowed regions (%)	2.4	6.1
generously allowed regions (%)	0.0	0.0

(b) *apo*-H91F CopC Protein

crystallization pH	6.6
radiation source	rotating anode
X-ray wavelength (Å)	1.5418
space group	$I4_1$
unit cell parameters	
a (Å)	72.3
c (Å)	47.5
mosaicity (deg)	0.44
resolution (Å)	30.0−2.0 (2.07−2.00)
unique observations	8189
total observations	19 972
completeness (%)	97.7 (95.6)
redundancy	2.4 (2.1)
$I/\sigma(I)$	23.8 (3.7)
R_{merge}[b]	0.038 (0.242)

Refinement Statistics

no. molecules/asu	1
resolution range (Å)	27.0−2.0
no. protein residues	97
no. of Cu atoms	0
no. of water molecules	63
no. of other entities	1 (Na^+)
total no. of atoms	835
reflections	8184
R_{cryst}[c]	0.175 (0.208)
R_{free}[c,d]	0.213 (0.346)
rms Δ − bond lengths (Å)	0.010
rms Δ − bond angles (deg)	1.384
average protein *B*-value (Å^2)	46.9
ESU (Å)[e]	0.10
Ramachandran plot, residues in: [f]	
most favored regions (%)	96.2
additional allowed regions (%)	3.8
generously allowed regions (%)	0.0

[a] Values in parentheses are for the highest resolution shell. [b] $R_{merge} = \sum|I_h - \langle I_h\rangle|/\sum\langle I_h\rangle$. [c] R values $= \sum|F_{obsd} - F_{calcd}|/\sum F_{obsd}$. [d] 5% of the reflections were reserved for the calculation of R_{free}. [e] Estimated standard uncertainty in atomic position, based on maximum likelihood.[36] [f] Calculated using PROCHECK.[54]

Table 4. Interatomic Distances (Å) and Angles (deg) Involving Copper Ions for $Cu^{I}Cu^{II}$-CopC Proteins

Low pH Form	
Distance (Average for Molecules A, B, and C)	
Cu^{I}−Met 43 S^{δ} [a]	2.4(2)
Cu^{I}−Met 46 S^{δ} [a]	2.2(2)
Cu^{I}−Met 40 S^{δ} [b]	2.4(2)
Cu^{I}−Met 51 S^{δ} [b]	2.3(2)
Cu^{II}−His 1 $N^{\epsilon 2}$	2.3(2)
Cu^{II}−His 91 $N^{\delta 1}$	2.0(2)
[c] Cu^{II}−His 48** $N^{\epsilon 2}$	2.2(2)
Cu^{II}−OH_2	2.5(2)
Angle (Average for Molecules A, B, and C)	
Met 43 S^{δ} > Cu^{I} > Met 46 S^{δ} [a]	118
Met 43 S^{δ} > Cu^{I} > Met 40 S^{δ} [a,b]	105
Met 43 S^{δ} > Cu^{I} > Met 51 S^{δ} [a,b]	107
Met 46 S^{δ} > Cu^{I} > Met 40 S^{δ} [a,b]	107
Met 46 S^{δ} > Cu^{I} > Met 51 S^{δ} [a,b]	108
Met 40 S^{δ} > Cu^{I} > Met 51 S^{δ} [b]	108
His 1 $N^{\epsilon 2}$ > Cu^{II} > His 91 $N^{\delta 1}$	159
His 1 $N^{\epsilon 2}$ > Cu^{II} > His 48** $N^{\epsilon 2}$ [c]	101
His 1 $N^{\epsilon 2}$ > Cu^{II} > OH_2	76
His 91 $N^{\delta 1}$ > Cu^{II} > His 48** $N^{\epsilon 2}$ [c]	95
His 91 $N^{\delta 1}$ > Cu^{II} > OH_2	85
His 48** $N^{\epsilon 2}$ > Cu^{II} > OH_2 [c]	168
High pH Form	
Distance	
Cu^{I} −His 48 $N^{\epsilon 2}$	2.04(8)
Cu^{I}−Met 40 S^{δ}	2.40(8)
Cu^{I}−OH_2	2.47(8)
Cu^{I} − Cu^{I}* [d]	4.81(8)
Cu^{II}−His 1 N	2.18(8)
Cu^{II}−His 1 $N^{\delta 1}$	1.96(8)
Cu^{II}−His 91 $N^{\delta 1}$	1.95(8)
Cu^{II}−OH_2	1.82(8)
Angle	
His 48 $N^{\epsilon 2}$ > Cu^{I} > Met 40 S^{δ}	118
His 1 N > Cu^{II} > His 1 $N^{\delta 1}$	98
His 1 N > Cu^{II} > His 91 $N^{\delta 1}$	152
His 1 N > Cu^{II} > OH_2	95
His 1 $N^{\delta 1}$ > Cu^{II} > His 91 $N^{\delta 1}$	102
His 1 $N^{\delta 1}$ > Cu^{II} > OH_2	158
His 91 $N^{\delta 1}$ > Cu^{II} > OH_2	74

[a] For the Cu^{I} atom belonging to molecule A, B, or C, Met 43 and Met 46 also belong to molecules A, B, and C, respectively. [b] For the Cu^{I} atom belonging to molecules A, B, or C, Met 40 and Met 51 belong to molecules B, A, and C* (generated by symmetry operation $x - y, -y, -z + {}^{1}/_{3}$), respectively. [c] For molecules A, B, and C, His 48** belongs to molecules A**, B**, or C**, generated by symmetry operations $-y, x - y, z + {}^{2}/_{3}$; $-x + y, -x, z + {}^{1}/_{3}$ and $-x + y, -x, z + {}^{1}/_{3}$, respectively. [d] Cu^{I}* belongs to molecule A*, generated by symmetry operation $-y, -x, -z + {}^{1}/_{2}$.

and the refinement was completed using Refmac5 with TLS.[41] For all structures, water molecules were added automatically using ARP/wARP and confirmed by inspection of electron density maps in O after consideration of conservative hydrogen-bonding criteria.[35,42]

Relevant interatomic distances and angles for the copper centers are provided in Table 4 for each of the $Cu^{I}Cu^{II}$-CopC structures.

Results and Discussion

Expression, Purification, and Characterization of Wild-Type and Variant CopC Proteins. CopC was expressed in *E. coli* as the *apo*-protein. It is slightly basic with a predicted charge of +1 at pH 7. Consequently, it binds weakly to cation-exchange resins but does not bind to anion-exchange resins, allowing ready purification by conventional chromatography. The predicted positive charge increases as metal atoms bind, allowing ready separation and analysis of different forms of the protein.

Scheme 2

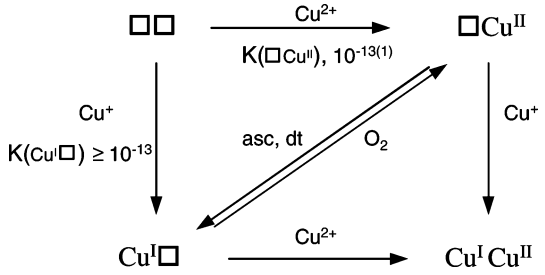

Generation and isolation of various metalated forms of the CopC protein are documented below and in Table 2. For efficient notation for the wild-type protein, an empty copper site is indicated by □. Hence the *apo* form is □□, the half-loaded forms are Cu^{I}□ and □Cu^{II} and the fully loaded form is $Cu^{I}Cu^{II}$. Equivalent notation applies to the Hg^{II} derivatives and the variant forms.

Addition of Cu^{2+} solution converted *apo*-CopC (□□) to a stable Cu^{II} form □Cu^{II} which, after removal of weakly bound Cu^{2+} by gel filtration, contained a single equivalent of Cu^{II} (Table 2, entry 3). Subsequent addition of Cu^{+} as $[Cu^{I}(MeCN)_4]^{+}$ followed by gel filtration produced a second copper form, $Cu^{I}Cu^{II}$. Analysis for Cu^{I} with the colorimetric reagent bcs in the absence and presence of reductant NH_2OH confirmed the stoichiometry as 2 equiv of copper (one as Cu^{I}, the second as Cu^{II}; Table 2, entry 2). The same $Cu^{I}Cu^{II}$ form was generated by the addition of 2 equiv of Cu^{2+} in the presence of NH_2OH. In the absence of this weak reductant, □Cu^{II} was the only isolable protein. These experiments confirm that there are two distinct copper sites in CopC: one is specific for Cu^{I}, and the other, for Cu^{II}.[14]

Metalated derivatives containing bound Cu^{II} (□Cu^{II} and $Cu^{I}Cu^{II}$) were stable in air. Addition of 1 or 2 equiv of Cu^{+} to □□ in air led to the clean isolation (> 90% yield) of □Cu^{II} or $Cu^{I}Cu^{II}$, respectively. Exposure of □□ to Cu^{+} under anaerobic conditions generated Cu^{I}□ with an empty Cu^{II} site. This form was not stable in air, oxidizing rapidly and cleanly to □Cu^{II}. On the other hand, □Cu^{II} was converted to Cu^{I}□ in the presence of stronger reductants such as ascorbate and dithionite. These copper transfer reactions are summarized in Scheme 2 and explored in more detail below.

NMR and EXAFS structural data suggested that a Cu^{II}(His1)(His91)(Asp89)(Glu27)(OH_2) coordination site is present in □Cu^{II}.[13,14] Indeed, mutation of His1 to Phe diminished Cu^{II} binding to the extent that the Cu^{II}-H1F form was unable to survive gel filtration. The *apo* form of this H1F variant with a disabled Cu^{II} site is designated by □X. Cu^{I}X is generated by addition of Cu^{+} to □X or by reduction of the H1F protein □Cu^{II}. In contrast to Cu^{I}□, Cu^{I}X is stable in air. Mutation of His91 to Phe also weakens Cu^{II} binding but to a lesser extent (the *apo* protein H91F is denoted by □$^{\downarrow}$). On the other hand, mutation of the proposed Cu^{II} ligand Glu27 to generate variant E27G actually increased the affinity for Cu^{II} slightly (*apo* form is denoted by □$^{\uparrow}$). It is apparent that the chemistries of the two copper binding sites in CopC are interdependent. Quantitative details are provided below.

(40) Murshudov, G. N.; Vagin, A. A.; Dodson, E. J. *Acta Crystallogr., Sect. D: Biol. Crystallogr.* **1997**, *53*, 240−255.
(41) Winn, M. D.; Isupov, M. N.; Murshudov, G. N. *Acta Crystallogr., Sect. D: Biol. Crystallogr.* **2001**, *57*, 122−133.
(42) Lamzin, V. S.; Wilson, K. S. *Acta Crystallogr., Sect. D: Biol. Crystallogr.* **1993**, *49*, 129−147.

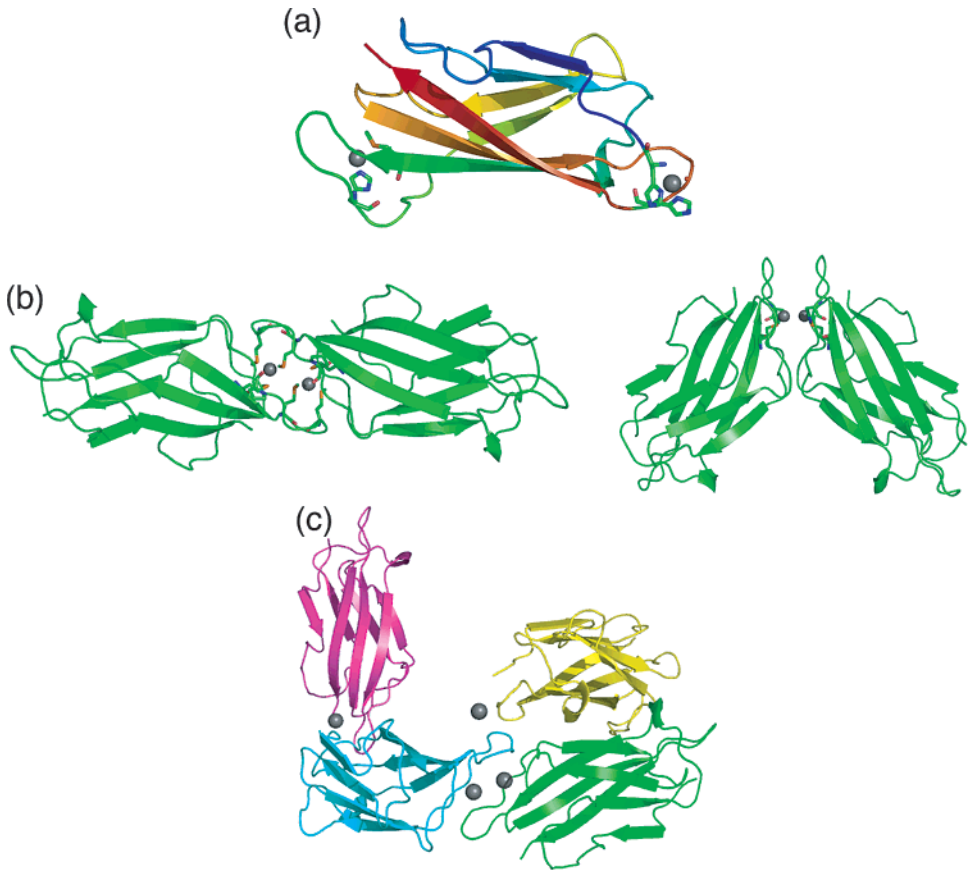

Figure 5. Crystal structures of $Cu^{I}Cu^{II}$-CopC. The positions of the copper atoms are indicated by gray spheres. Ligating residues are highlighted. (a) Ribbon representation of a $Cu^{I}Cu^{II}$-CopC molecule from the high pH structure ($P4_32_12$). The molecule is shaded from blue at the N-terminus to red at the C-terminus. (b) Cu^{I}-linked CopC dimers from the low pH ($P3_221$, left) and high pH ($P4_32_12$, right) structures. (c) Copper "sharing" within the low pH ($P3_221$) crystal structure. Molecule A (blue) is shown sharing a total of 4 × 0.5 Cu atoms with molecules B (green, Cu^{I}-linked dimer), A** (pink, Cu^{II}-linked dimer; related by symmetry operation $-y, x - y, z + {}^{2}/_{3}$) and A*** (yellow, Cu^{II}-linked dimer; related by symmetry operation $-x + y, -x, z + {}^{1}/_{3}$).

Table 5. Sedimentation Equilibrium Data for the Wild-Type *apo*- and $Cu^{I}Cu^{II}$-CopC Proteins[a]

protein	pH	buffer (50 mM; NaCl, 100 mM)	molar mass exptl (Da)	molar mass theor. (Da)	baseline
□□	7	KPi	11 600	10 534	0.034
$Cu^{I}Cu^{II}$	7	KPi	11 500	10 661	0.031
$Cu^{I}Cu^{II}$	4.5	NaAc	11 000	10 661	0.006

[a] Concentration, 60 mM; OD ≈ 0.5.

□□ fluoresced intensely with a maximum at 320 nm when excited at 280 nm (Figure 4a), a property attributable to the unique tryptophan residue W83 located between the two metal binding sites and about 10 Å from the Cu^{II} site (Figure 1). Bound Cu^{II} but not Cu^{I} quenched the fluorescence intensity linearly until 1 equiv of Cu^{II} was bound (Figure 4b(i)). This provided a convenient probe for monitoring Cu^{II} transfer reactions.

All forms of CopC examined by analytical gel-filtration (□□, □Cu^{II}, $Cu^{I}Cu^{II}$, and $Cu^{I}X$) eluted indistinguishably from the column in the pH range 4.5−7.5. The elution volumes are consistent with monomeric protein molecules in solution (Figure S3; Table 2, entry 11). This conclusion is supported by sedimentation equilibrium analysis of selected species (Table 5).

X-ray Crystallography. Crystals of the $Cu^{I}Cu^{II}$ form of wild-type CopC were grown in two forms from the same protein sample. The low pH form crystallized at pH ∼4.6, and the structure was solved and refined in space group $P3_221$ (2.25 Å resolution, three molecules/asu: A, B, and C). For this structure, the positions of six Cu atoms per asymmetric unit were determined experimentally by SAD phasing using data collected at a single wavelength, close to the Cu K-edge. The model also includes 4 NO_3^- ions, originating from the main component of the crystallization solution, ammonium nitrate. The superposition of molecules B or C onto molecule A gave an rmsd for the positions of 102 Cα atoms of 0.29 and 0.22 Å, respectively. This is consistent with the fact that NCS restraints were removed in the final refinement cycles and with the ESU of the structure (0.18 Å; Table 3).

The high pH form crystallized at pH ∼7.5 and was solved and refined in space group $P4_32_12$ (1.60 Å resolution, one molecule/asu) by molecular replacement, using a single molecule from the low pH structure as a search model. The locations of 2 Cu atoms per asymmetric unit were assigned by inspection of anomalous difference Fourier maps. The positions later attributed to Cu^{I} and Cu^{II} sites corresponded to 7.0 and 4.5 σ peaks, respectively, in these maps. As expected from the relative Cu and S anomalous scattering factors at Cu Kα radiation, the peak heights for the Cu sites were comparable to those corresponding to the methionine S^{δ} positions (4.5−5.5 σ). The statistics for both the low and high pH structures are given in Table 3. Both refined to *R*-factors < 20% and have excellent stereochemistry. A ribbon representation is presented in Figure

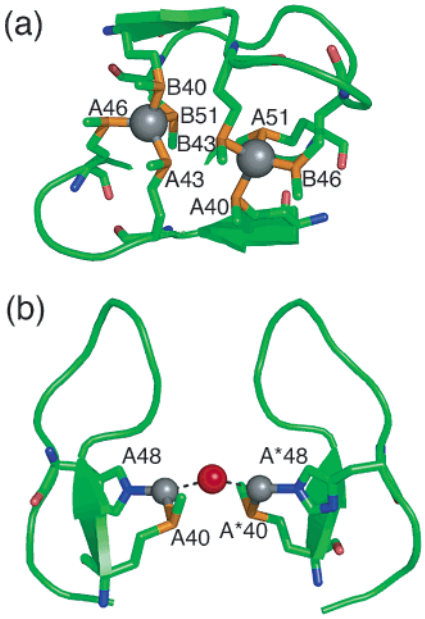

Figure 6. Cu^{I} binding sites in crystals of $Cu^{I}Cu^{II}$-CopC. (a) low pH form (space group, $P3_221$); (b) high pH form (space group, $P4_32_12$). Water molecule W1 lies on a crystallographic two-fold axis. Ligand residues are labeled. Copper atoms are represented as gray spheres.

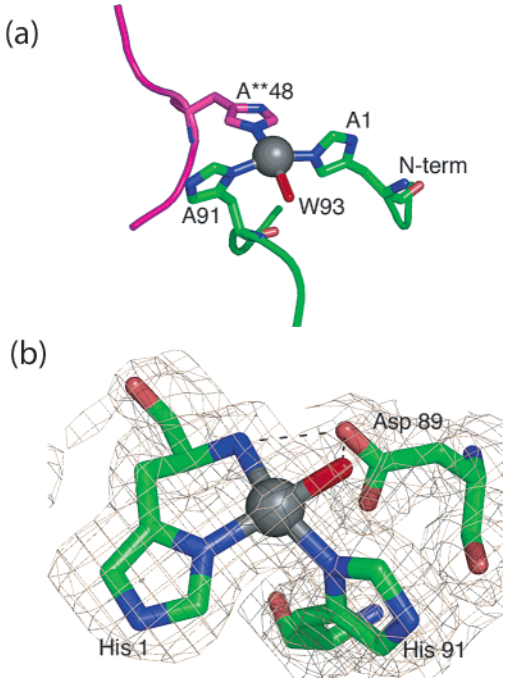

Figure 7. Cu^{II} binding sites in crystals of $Cu^{I}Cu^{II}$-CopC. (a) Low pH form (space group, $P3_221$). Molecule A is represented in green and A** (generated by symmetry operation $-y, x - y, z + {}^{2}/_{3}$) in pink. (b) High pH form (space group, $P4_32_12$). $2F_o-F_c$ density is represented as a gray net. The copper atoms are depicted as gray spheres.

5a. A full account of each of the structures is provided in the Supporting Information. A briefer summary is presented here.

Structure of $Cu^{I}Cu^{II}$-CopC Crystallized at pH ~4.6 (Low pH Form). Cu^{I}-Linked Molecules. There are three molecules A, B, and C in the asymmetric unit of this $P3_221$ structure. They are arranged in head-to-head dimers, linked by two copper atoms proposed to be Cu^{I} (Figure 5b, left-hand side). The average buried surface for the Cu^{I}-linked dimers is approximately 10% of the total surface area of the monomeric protein. In the case of the A/B Cu^{I}-linked dimer, one Cu^{I} ion is coordinated by Met residues A43, A46, B40, and B51 (Figure 6a) while the second Cu^{I} atom is coordinated by Met residues A40, A51, B43, and B46. The average Met $S^{\delta}-Cu^{I}$ distance for the three Cu^{I} ions in the asymmetric unit is 2.3(2) Å. Each Cu^{I} ion lies in an approximately tetrahedral geometry with an average Met S^{δ} > Cu^{I} > Met S^{δ} angle of 109° (Table 4). A search of the Metalloprotein Database (http://metallo.scripps.edu) indicates that these are the first protein tetrathioether-metalate centers to have been characterized crystallographically.[43]

Cu^{II}-Linked Molecules. Each molecule in the asymmetric unit (molecules A, B, C) is bridged to its symmetry-related partner by a copper atom proposed to be Cu^{II}. For example, the Cu^{II} ion bound to molecule A is in a four-coordinate tetragonal environment bound by residues His A1, His A91, His A**48 (generated by symmetry operation $-y, x - y, z + {}^{2}/_{3}$), and water molecule W 93 (Figure 7a). The average His $N^{\epsilon}-Cu^{II}$ and H_2O-Cu^{II} bond lengths for the three Cu^{II} atoms in the asymmetric unit are 2.2(2) and 2.5(2) Å, respectively (Table 4). The average His N^{ϵ} > Cu > His N^{ϵ} angle is 98°, indicating an approximately square-planar coordination geometry.

In summary, these crystals are composed of an infinite Cu^{I}/Cu^{II}-linked polymer of CopC monomers (Figure 5c). Every molecule A is linked to molecule B through two Cu^{I} atoms and to molecules A** and A*** through single Cu^{II} atoms (Figures 5−7). Molecules B and C are linked in equivalent ways (see Supporting Information). There are 4 × 0.5 Cu atoms associated with each CopC molecule, i.e., a Cu:protein stoichiometry of 2:1.

Structure of $Cu^{I}Cu^{II}$-CopC Crystallized at pH ~7.5 (High pH Form). Cu^{I}-Linked Molecules. The single CopC molecule in this model lies close to the crystallographic two-fold axis, so that a pair of CopC molecules A and A* is generated by symmetry operation $-y, -x, -z + {}^{1}/_{2}$. Two copper atoms (proposed to be Cu^{I}) are found at the dimer interface in an arrangement depicted in Figures 5b (right-hand side) and 6b. The buried surface area between CopC molecule A and A* is approximately 13% of the total surface area of each monomer.

Each Cu^{I} ion is coordinated by Met 40 (Met 40 S^{δ} − Cu = 2.40(8) Å) and His 48 (His 48 $N^{\epsilon 2}$ − Cu = 2.04(8) Å) with a S > Cu > N bond angle of 118°. A search of the Cambridge Data Base (CDB) for molecules containing both $Cu^{I}-SR_2$ and $Cu^{I}-N$ bonds revealed respective ranges of 2.26−2.37 and 1.91−2.02 Å.[44−47] Water molecule W1 lies directly on the crystallographic two-fold axis between the Cu^{I} ions, providing a distorted trigonal environment (Met 40 S^{δ} > Cu^{I} > His 48 $N^{\epsilon 2}$ = 118°; His 48 $N^{\epsilon 2}$ > Cu^{I} > W1 = 151°; Met 40 S^{δ} > Cu^{I} > W1 = 92°). The Cu−W1 distance is 2.47(8) Å. The above CDB search also revealed a range of $Cu^{I}-OH_2$ distances of 2.20−2.24 Å. Consequently, the Cu−W1 distance is very long for a direct coordinate bond.

(43) Castagnetto, J. M.; Hennessy, S. W.; Roberts, V. A.; Getzoff, E. D.; Tainer, J. A.; Pique, M. E. *Nucleic Acids Res.* **2002**, *30*, 379−382.
(44) Olmstead, M. M.; Musker, W. K.; Kessler, R. M. *Transition Met. Chem. (Dordrecht, Neth.)* **1982**, *7*, 140−146.
(45) Diaddario, L. L., Jr.; Dockal, E. R.; Glick, M. D.; Ochrymowycz, L. A.; Rorabacher, D. B. *Inorg. Chem.* **1985**, *24*, 356−363.
(46) Donlevy, T. M.; Gahan, L. R.; Hambley, T. W.; Hanson, G. R.; Markiewicz, A.; Murray, K. S.; Swann, I. L.; Pickering, S. R. *Aust. J. Chem.* **1990**, *43*, 1407−1419.
(47) Chou, J.-L.; Chyn, J.-P.; Urbach, F. L.; Gervasio, D. F. *Polyhedron* **2000**, *19*, 2215−2223.

The Cu^{II} Site. A single CopC molecule donates all the protein ligands for the copper atom proposed to be Cu^{II}. The distorted tetragonal site is provided by the amino terminus of the protein (His 1 N−Cu^{II} = 2.18(8) Å), the side chains of His 1 (His 1 $N^{\delta 1}$−Cu^{II} = 1.96(8) Å) and His 91 (His 91 $N^{\delta 1}$−Cu^{II} = 1.95-(8) Å), and a water molecule (W78−Cu^{II} = 1.82(8) Å) (Figure 7b). Asp 89 makes a hydrogen bond to ligand W78 (Asp 89 $O^{\delta}2$−W78 = 2.14(8) Å) and to the amino terminus ligand His 1 N (Asp 89 $O^{\delta}2$−His 1 N = 2.70(8) Å).

The temperature factors associated with constituents of the Cu^{II} site are higher than the average temperature factor of the structure (average *B* factor for (i) ligand atoms ∼29 $Å^2$; (ii) Cu^{II} atom = 28 $Å^2$; (iii) structure (main chain atoms only) = 21 $Å^2$). In fact, the Cu^{II} atom has been modeled with an occupancy of 0.75. The assignment of Cu^{II} occupancies > 0.75 gave models with unacceptably high *B* factors for the Cu^{II} atom and significant negative density in difference Fourier electron density maps at this position. This is consistent with the smaller peak height observed in the anomalous difference Fourier map for this Cu^{II} atom compared to the Cu^{I} position (4.5 and 7.0 σ, respectively). Instability in the refinement of the structure of the Cu^{II} site was addressed by introducing restraints for the Cu^{II}−W78 and W78−Asp 89 $O^{\delta 2}$ distances. Although the structure of the Cu^{II} site is consistent with the interpretation of the electron density maps, the Cu^{II}−W78 and W78−Asp 89 $O^{\delta 2}$ distances are shorter than expected. This indicates some degree of disorder associated with this Cu^{II} site.

Structure of the apo-H91F Protein. The H91F protein crystallized in space group $I4_1$, with one molecule per asymmetric unit. The structure was solved using the coordinates of the $Cu^{I}Cu^{II}$ high pH form as the search model, omitting His 91. Difference Fourier electron density maps, calculated following initial refinement of the molecular replacement solution, clearly showed the H91F variation. Importantly, an anomalous difference Fourier map, calculated at the same stage, showed a single significant peak only (ca. 4.0 σ), corresponding to the position of the S^{γ} atom of Met 66. No peaks assignable to Cu positions were observed. The crystals were therefore composed of *apo*-H91F-CopC. The absence of Cu from the H91F structure is consistent with the presence of edta in the crystallization solution and with the determined Cu binding constants. In addition, electron density maps in the region of the 40−51 Cu-binding loop were disordered. Consequently, residues 45−49 were omitted from the final model. No significant oligomeric associations of CopC molecules were observed in the crystal packing of the *apo*-H91F structure.

Superposition of the *apo*-H91F structure onto the low pH and high pH $Cu^{I}Cu^{II}$-CopC structures gives an rmsd for the positions of 97 common Cα atoms of 0.58 (average of molecules A, B, and C) and 0.59 Å, respectively. Despite the lack of Cu^{I} and Cu^{II}, the overall structure is essentially conserved in this mutant. In fact, the large majority of the side chain conformations are identical for the high pH $Cu^{I}Cu^{II}$ and *apo*-H91F structures. The largest difference when the two structures are superimposed is that between the positions of the Cα atoms of His 1 (2.5 Å). The amino terminus lies closer to the 85−93 Cu-binding loop in the *apo*-His91F structure than it does in the Cu-loaded CopC structures. The side chains of both Glu 27 and Asp 89 hydrogen bond to His 1 (Glu 27 $O^{\epsilon}1$−His 1 N = 2.8 Å; Asp 89 $O^{\delta}2$−His 1 N = 2.7 Å) (Figure 8). The equivalent

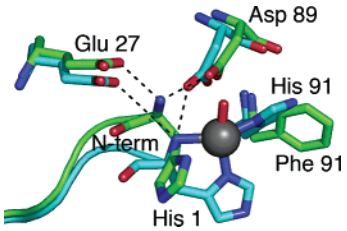

Figure 8. Hydrogen bonding between Glu 27 and the N-terminus in *apo*-H91F and comparison with the high pH $Cu^{I}Cu^{II}$-CopC structure. The H91F (green) and high pH (teal) structures are superposed. Hydrogen-bonding interactions among Glu 27, Asp 89, and the N-terminus are indicated. For clarity, the Cu^{II} site of the high pH structure is represented, with the Cu atom as a gray sphere.

distances in the low pH (average) and high pH $Cu^{I}Cu^{II}$ structures are 3.7 Å (Glu 27), 12.3 Å (Asp 89) and 4.2 Å (Glu 27), 2.7 Å (Asp 89), respectively. Asp 89 also hydrogen bonds to the aqua ligand in the high pH form (Figures 7b, 8). In native CopC, Glu 27 and Asp 89 probably compete with Cu^{II} for the amino terminus. In fact, mutation of Glu 27 increases the affinity of the variant form E27G for Cu^{II} (see below).

Comparison of the Two $Cu^{I}Cu^{II}$-CopC Structures. The essential molecular structure is similar in both crystalline forms (pH ∼4.6, $P3_221$ and pH ∼7.5, $P4_32_12$; Figure 5a). In addition, each molecule in each structure is bound to a total of two Cu atoms. The Cu−Cu distances are approximately 30 Å. In both space groups, Cu atoms are bound at the interface between Cu-linked pairs of molecules. However, the structures reported here differ in three ways: (1) the coordination chemistry at each Cu site, (2) the conformations of loops which provide the Cu ligands, and (3) the modes of interaction between CopC molecules.

Superposition of the single CopC molecule from the $P4_32_12$ structure (high pH) onto molecule A of the $P3_221$ structure (low pH) gives an rmsd for 102 Cα atoms of 0.93 Å. This is well outside the accumulated positional error for the two structures. Examination of a plot of change in Cα position versus residue number shows that the positions of the main chain atoms for residues 44−49 and 88−91 are significantly different. The largest differences are for residues Glu 47 (Cα separation of 3.6 Å) and Asp 89 (Cα separation of 2.8 Å).

Residues 44−49 and 88−91 comprise parts of loops (residues 40−51 and 85−93), which connect the ends of strands that make up the Greek key β-barrel fold. These may be described as copper-binding loops as, apart from His 1, they include all residues observed to bind to Cu atoms in the two structures (Met 40, 43, 46, 51, His 48, His 91).

These loops also differ in the conformations of their side chains and associated torsion angles. Figure S4 shows a difference Ramachandran plot comparing the torsion angles of molecule A of the low pH structure and the single molecule of the high pH structure. The positional differences in the 40−51 loop are accompanied by changes in torsion angles. The loop comprised of residues 85−93 shows similar conformational variations. In all cases, conformational changes move the torsion angles of these residues from one allowed region of the Ramachandran plot to another, indicating different but allowed secondary structures.

These changes in the structures of the Cu-binding loops are accompanied by changes in the coordination geometries and in the nature of the ligands. For example, in the low pH structure,

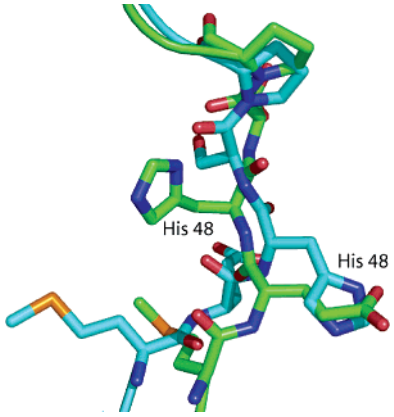

Figure 9. Relative conformations of His 48. The high pH and low pH $Cu^{I}Cu^{II}$-CopC structures are represented in green and blue, respectively.

His 48 is a ligand to Cu^{II}, participating in a Cu^{II}-linked dimer with a symmetry-related neighboring molecule (Figure 7a). In contrast, in the high pH structure, His 48 is a ligand to Cu^{I} (Figure 6b). The conformational changes to the 40−51 loop necessary for such variation are shown in Figure 9: the directions of the His 48 side chains vary by ∼180°. In the low pH structure, four out of the five Met residues (Met 40, 43, 46, 51) are Cu^{I} ligands (Figure 6a), whereas only Met 40 is a Cu^{I} ligand in the high pH structure (Figure 6b). In the latter case, Met 43, 46, 51 form part of the A/A* dimer interface, generated by the crystallographic two-fold axis. In both structures, the side chains of His 1 and His 91 are Cu^{II} ligands (Figure 7). The N-terminal nitrogen atom is a Cu^{II} ligand in the high pH structure (pH ∼7.5) but not in the low pH structure (pH ∼4.6). This may be related to a pK_a of about 8 for this functional group, allowing protons to compete with Cu^{II} at pH ∼4.6.

Comparison of $Cu^{I}Cu^{II}$-CopC, *apo*-H91F CopC, and *apo*-PcoC Structures. Both $Cu^{I}Cu^{II}$CopC structures reported here confirm the overall Greek key β-barrel structure defined for *apo*-CopC by NMR (Figure 5a).[13] Superposition of the high pH or low pH structures with the average *apo*-CopC structure as determined by NMR (PDB code 1M42) gives an rmsd in 102 common Cα positions of 2.6 and 2.7 Å, respectively. These are significant differences. The respective rmsd values decrease to 2.0 and 2.1 Å if the copper-binding loop residues 40−51 and 85−93 are omitted from the superposition. It should be noted that we were unable to solve either CopC structure by molecular replacement using the NMR structure as a search model. The large differences in backbone structure between that determined by NMR and X-ray diffraction are consistent with this observation.

Sharing of Cu between CopC monomers in Cu-linked dimers, as observed in the $Cu^{I}Cu^{II}$ structures presented here, was not detected in the NMR experiments. Dimerization and metal-sharing are commonly observed in X-ray structures of metal-trafficking proteins. For example, the $[Cu^{I}(S-Cys)_4]^{3-}$ center present in a crystalline form of the human cytosolic copper chaperone Atox1 (Hah1) bridged two protein molecules, each of which contributed two S−Cys ligands.[48] A detailed comparison of the CopC and PcoC structures (67% sequence homology; Figure 2) is presented in the Supporting Information.

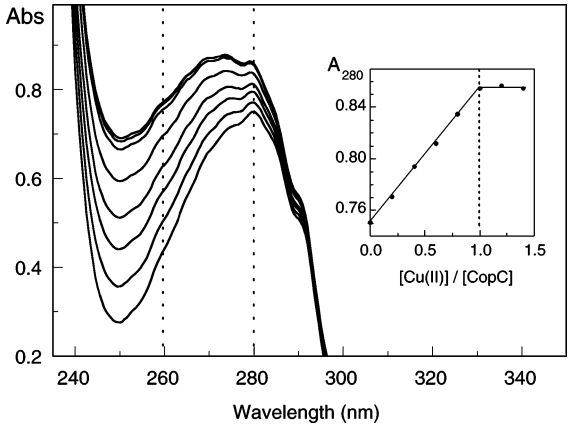

Figure 10. Change in UV spectrum upon titration of *apo*-CopC □□ (86 μM in 1.0 cm cell) in mes buffer (20 mM; pH 6.0) with $CuSO_4$ (1.72 mM). Insert shows plot of A_{280} versus [Cu(II)]/[□□].

Interestingly, despite attempts to crystallize Cu^{I}- and Cu^{II}-loaded PcoC, in addition to soaking crystals in $CuSO_4$ (aerobic) or CuCl (anaerobic), no copper could be detected in either of the PcoC structures.[16] The *apo*-PcoC protein, as expressed, features Ala as the N-terminal residue rather than the His residue that is presumably present in the native protein (Figure 2); i.e., the equivalent of His 1 in the CopC protein crystallized here was His 2 in the PcoC protein. Native PcoC was crystallized at pH 7.5 and, if analogous to the high pH CopC structure presented here, would have been expected to bind Cu^{II} at its N-terminus, using both the His 1 side chain and N-terminus as Cu^{II} ligands. The presence of the additional N-terminal Ala residue in PcoC may have weakened Cu^{II} binding.[49] Such a possibility is consistent with the properties of the CopC variant H1F discussed below.

The Metal-Binding Sites in CopC Are Specific for Cu^{I} and for Cu^{II}. Addition of Cu^{2+} solution to *apo*-CopC (□□; 86 μM) induced an increase in absorbance around 260 nm (Figure 10), plausibly assigned to ligand His → Cu^{II} charge-transfer transitions originating from ligands H1 and/or H91 (Figure 7b). There was a clear endpoint at Cu: □□ = 1:1 (inset, Figure 10), and the stable half-loaded form □Cu^{II} was formed (Table 2, entry 3). Addition of $[Cu^{I}(MeCN)_4]^{+}$ solution to □Cu^{II} induced a further slight increase in that absorbance (Table 1), and a new stable species $Cu^{I}Cu^{II}$ was isolated from the solution (Table 2, entry 2). Likewise, addition of 1 equiv of Cu^{+} to the *apo*-H1F protein □X also induced a similar small increase in absorbance around 260 nm (Table 1) with isolation of stable Cu^{I}X (Table 2, entry 5). These experiments further demonstrate the presence of two distinct metal-binding sites in CopC that are specific for Cu^{I} and Cu^{II}, respectively.

Addition of Hg^{2+} solution to either □Cu^{II} or □□ (120 and 150 μM, respectively; 10 mM mes; pH 6.0) also induced an increase in absorbance in the near-ultraviolet region with apparent endpoints at Hg:CopC = 1:1 or 2:1, respectively (Figure 11). Note that the molar absorbance change was the same for each protein (Figure 11b,c). On the other hand, addition of Hg^{2+} to the $Cu^{I}Cu^{II}$ protein solution caused no change in the absorbance. These results led to two conclusions: (i) Hg^{II} can bind at or near to both metal-binding sites in CopC, but binding can be blocked by bound Cu^{I} and/or Cu^{II}; (ii) the Hg^{2+}

(48) Wernimont, A. K.; Huffman, D. L.; Lamb, A. L.; O'Halloran, T. V.; Rosenzweig, A. C. *Nat. Struct. Biol.* **2000**, *7*, 766−771.

(49) Djoko, K.; Xiao, Z.; Huffman, D. L.; O'Halloran, T. V.; Wedd, A. G. Unpublished observations.

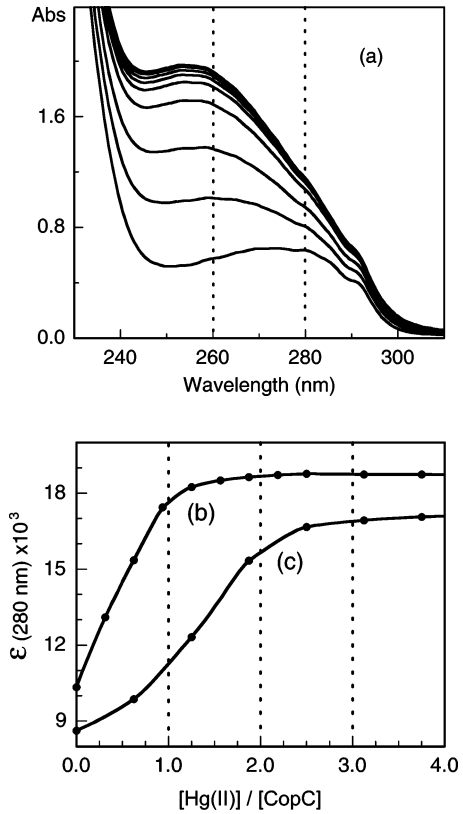

Figure 11. (a) Change in UV spectrum upon titration of Cu^{II}-CopC $\square Cu^{II}$ (120 μM in 0.5 cm cell) in mes buffer (20 mM; pH 6.0) with $Hg^{II}Cl_2$; Plots of molar absorbance at 280 nm versus (b) $[Hg^{II}]/[\square Cu^{II}]$ for the above titration (a); (c) $[Hg^{II}]/[\square\square]$ for the equivalent titration with *apo*-CopC $\square\square$ (150 μM in 0.5 cm cell).

probe reports binding of Hg^{2+} at or near the Cu^{I} site *only* via ligand His and/or Met $\rightarrow$ Hg^{II} charge-transfer transitions (cf. Figure 6).

The two bound Hg^{II} ions can be displaced by sequential addition of Cu^{2+} and Cu^{+} or vice versa as demonstrated by the experiments reported in Figures 12 and S7. The observed values of ΔA_{280} are within experimental error of those predicted from the ϵ_{280} values listed in Table 1. Either of these procedures leads to the $Cu^{I}Cu^{II}$ form, free of Hg^{2+} following gel filtration (Scheme 2). It is apparent that excess Hg^{2+} does not inhibit binding of Cu^{2+} and Cu^{+} nor do either of these ions inhibit binding of the other. Addition of Zn^{2+} or Cd^{2+} to an equivalent solution of Hg^{2+}: $\square\square$ = 3:1 caused no change in absorbance. These ions cannot compete with Hg^{2+} for the Cu^{I} site.

Estimation of Metal Dissociation Constants. Hg^{II} Dissociation Constants. Titration of Hg^{2+} into $\square Cu^{II}$ (120 μM) caused a linear increase in absorbance at 280 nm with an apparent endpoint at Hg^{II}/CopC = 1 (Figure 11a,b), consistent with occupation of the Cu^{I} site by Hg^{II}. The equivalent titration at the lower concentration of $\square Cu^{II}$ (60 μM) led to a less well-defined endpoint. This observation suggested a dissociation constant $K_D(HgCu^{II})$ of about 10^{-6} M for Hg^{II} bound at or near to the Cu^{I} site (eq 4):

$$Hg^{II}Cu^{II} \leftrightarrow Hg^{2+} + \square Cu^{II}$$
$$K_D(HgCu^{II}) = \frac{[Hg^{2+}][\square Cu^{II}]}{[Hg^{II}Cu^{II}]} \approx 10^{-6}\,M \qquad (4)$$

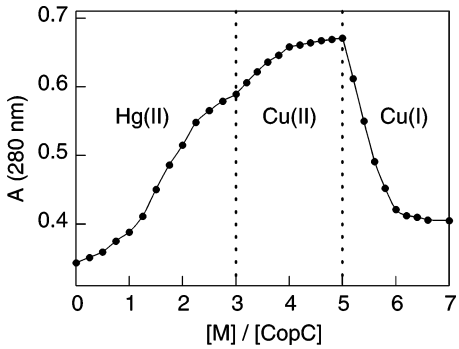

Figure 12. Changes in absorbance at 280 nm for $\square\square$ (78 μM) in mes (20 mM, pH 6.0) upon sequential titration with standardized solutions of Hg^{2+} (3 equiv), Cu^{2+} (2 equiv), and $[Cu(MeCN)_4]^{+}$ (2 equiv).

Addition of Hg^{2+} into either $\square Cu^{II}$ or $\square\square$ (120 and 150 μM, respectively; 10 mM mes; pH 6.0) led to the same molar absorbance change for each protein (Figure 11b,c). However, for $\square\square$, that increase was no longer linear and was extended to Hg^{2+}: $\square\square \approx 2$ with a less well-defined endpoint (compare Figure 11b,c). Since the absorbance change at 280 nm reports binding of Hg^{II} at or near the Cu^{I} site but not the Cu^{II} site, the observations suggest that Hg^{II} has a slightly higher affinity for the Cu^{II} site than for the Cu^{I} site (i.e., $K_D(Hg\square) \geq K_D(\square Hg)$). The well-defined endpoint in the titration of Hg^{II} into $\square Cu^{II}$ (Figure 11b) is consistent with the order

$$K_D(Hg\square) \geq K_D(\square Hg) \geq K_D(HgCu) \approx 10^{-6}\,M \qquad (5)$$

The presence of Cu^{II} at the Cu^{II} site appears to have increased the affinity for Hg^{II} at the Cu^{I} site (separated by about 30 Å). A similar effect was observed for Cu^{I} binding and is discussed below.

Cu^{I} Dissociation Constant. The affinity of the wild-type protein $\square\square$ for Cu^{I} was estimated via ligand competition with the ligand bcs (eq 1).[28] However, the affinity is outside the sensitive range of Cu^{I} detection by bcs ($\beta_2 = 10^{19.8}$). While a reproducible stepwise decrease in A_{483} (characteristic of $[Cu^{I}(bcs)_2]^{3-}$) was observed upon anaerobic addition of $\square\square$ (Figure 3), the practical imperatives (see Materials and Methods) permitted estimation of a minimum value only (highest possible affinity):

$$Cu^{I}\square \leftrightarrow Cu^{+} + \square\square$$
$$K_D(Cu^{I}\square) = \frac{[Cu^{+}][\square\square]}{[Cu^{I}\square]} \geq 10^{-13}\,M \qquad (6)$$

Other lines of evidences support a high affinity of Cu^{I} for $\square\square$: (i) the bound Hg^{II} at the Cu^{I} site ($K_D \sim 10^{-6}$ M) was displaced quantitatively by Cu^{+} (Figures 12 and S7); (ii) various Cu^{I} forms of CopC (e.g., $Cu^{I}Cu^{II}$, $Cu^{I}X$) could be isolated under aerobic conditions via cation exchange chromatography on Mono-S resin (see Figure 13b,e and discussion below). It appears that $K_D(Cu^{I}\square)$ lies in the range $10^{-7} \geq K_D(Cu^{I}\square) \geq 10^{-13}$ M.

Cu^{II} Dissociation Constants. The affinity of wild-type *apo*-CopC ($\square\square$) for Cu^{II} was estimated via ligand competition with egta as detailed in Materials and Methods. Linear quenching of CopC fluorescence upon Cu^{II} binding allowed quantitative monitoring of Cu^{II} occupancy in $\square\square$ as a function of total Cu^{II} concentration in the presence of fixed concentrations of CopC and egta. A plot of eq 3 for those experimental conditions where

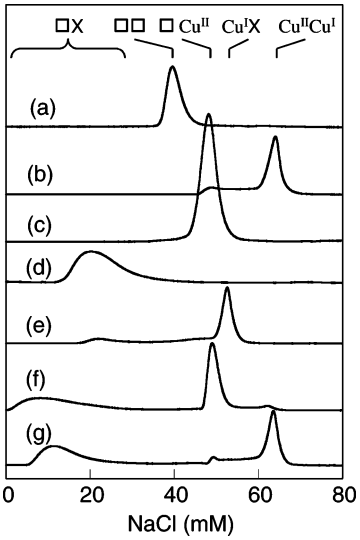

Figure 13. Elution profiles of CopC proteins (~60 μg) on a Mono-S HR5/5 cation exchange column (0.5 cm × 5 cm) in deoxygenated buffer (10 mM KPi; pH 7.0; NaCl gradient 0−80 mM). (a) □□; (b) Wild-type Cu^ICu^{II} (the increased absorption starting at the elution position of □Cu^{II} is due to slow oxidation of Cu^ICu^{II} by air promoted by the affinity of the Mono-S resin for Cu^{II} ions (cf. eq 9); (c) Wild-type □Cu^{II} (2 equiv) formed upon mixing □□ (1 equiv) with Cu^ICu^{II} (1 equiv) in air (eq 10); (d) H1F □X alone or a mixture of □X (1 equiv) and $Cu^{II}SO_4$ (2 equiv); (e) H1F Cu^IX formed upon mixing □X (1 equiv), $Cu^{II}SO_4$ (1.2 equiv), and NH_2OH (10 equiv); (f) □X and □Cu^{II} formed upon mixing Cu^IX (1 equiv) with □□ (1 equiv; cf. eq 11); (g) □X and Cu^ICu^{II} formed upon mixing Cu^IX (1 equiv) with □Cu^{II} (1 equiv) under anaerobic conditions (cf. eq 16).

Cu^{II} occupancy of *both* CopC and egta varied between 0.1 and 0.9 produced a straight line passing through the origin (Table 6; Figure 4c(i)). The slope provided reliable estimation of K_D-(□Cu^{II}) = $10^{-13(1)}$ M^{-1} (pH 7.0; I, 100 mM):

$$\square Cu^{II} \leftrightarrow Cu^{2+} + \square\square$$

$$K_D(\square Cu^{II}) = \frac{[Cu^{2+}][\square\square]}{[\square Cu^{II}]} = 10^{-13(1)}\,M \qquad (7)$$

This low value confirms tight binding of Cu^{II}. It is consistent with the observation of a defined endpoint at Cu^{2+}: □□ = 1:1 in the titration of □□ solution with Cu^{2+} when monitored by either fluorescence or absorption spectroscopy (Figures 4, 10). It is also consistent with the well-defined elution behavior of □Cu^{II} from a Mono-S cation exchange column (see Figure 13c and discussion below). Stronger Cu^{II} ligands such as edta ($K_A(Cu^{II}edta) = 3.2 \times 10^{15}$ M^{-1} at pH 7.0) remove bound Cu^{II} from CopC quantitatively (Figure 4b(ii)) but the reaction is slow (~12 h for completion).[50]

In the mononuclear Cu^{II} site of the high pH crystals, His1 provides both its imidazole and N-terminal amine functions as ligands (Figure 7b). Indeed, upon mutation of His1 to Phe, the affinity of the resultant variant protein H1F (□X) for Cu^{II} was diminished dramatically: (i) although titration of Cu^{2+} solution into □X still caused quenching of the W83 fluorescence emission and an increase in solution absorbance at 260 nm, the magnitudes of these changes were much smaller relative to those for □□ and there were no defined endpoints (Figure 4b(iv)); (ii) chromatography of a Cu^{2+}:□X = 1:1 solution on either gel-filtration or Mono-S cation exchange columns resulted in recovery of the *apo* form □X only (Figure 13d; Table 2, entry 4). These observations are consistent with a dissociation constant $K_D(\square Cu^{II}) > 10^{-5}$ M for the H1F variant, as estimated from experiments such as that in Figure 4b(iv). This estimate is in stark contrast with that derived for the wild-type protein (K_D-(□Cu^{II}) = $10^{-13(1)}$ M).

Residue His1 is effectively a bidentate ligand for the Cu^{II} ion in □Cu^{II} (Figure 7b). The benzyl side chain of phenylalanine in □X cannot act as a ligand, and its steric requirements may interfere with the ability of the amino terminus to act as a ligand. The mutation has converted the Cu^{II} center to an "adventitious" site in □X, incapable of selective binding of Cu^{2+} (His 91 remains as the only protein ligand). It is interesting to note that free histidine (with its ability to act as a bidentate or tridentate ligand to Cu^{II} via imidazole, amino, and carboxylato functions) binds Cu^{2+} at pH 7.4 with an apparent dissociation constant of $10^{-8.4}$ M, i.e., the approximate difference between those for wild-type CopC (10^{-13} M) and its H1F variant (10^{-5} M).[29,51]

His91 acts as a monodentate ligand for the Cu^{II} center via its imidazole side chain in both the high pH and low pH crystals (Figure 7). Indeed, mutation of His91 to Phe to provide the variant H91F (□↓) also diminished the affinity of CopC for Cu^{II} but to a lesser extent. As observed for the wild-type protein, clear endpoints at Cu^{2+}:□↓ = 1:1were detected in titrations of Cu^{2+} into □↓ by both fluorescence and absorbance spectroscopies (cf. Figures 4b(i) and 10). In addition, gel filtration of the above solutions to remove excess Cu^{2+} produced stable H91F protein □Cu^{II}. However, equivalent experiments involving competition between □↓ and egta for Cu^{2+} produced data equivalent to those given in Figure 4b(ii) for competition between □□ and edta. It was apparent that □↓ could not compete effectively with egta for Cu^{II} and has a lower affinity for Cu^{II} than does the wild-type protein □□. In addition, chromatography of H91F □Cu^{II} on the Mono-S cation exchange column provided two components, the □↓ and □Cu^{II} forms, with significantly increased absorption for the fractions eluted between these two components (Figure 14a). Apparently, the Mono-S resin competes effectively for Cu^{2+} ions with the □↓ protein (but not with the wild-type protein □□; cf. Figure 13c).

For protein variant E27G (□↑), experiments involving competition with egta for Cu^{II} led to a lower slope for eq 3 than that of the wild-type protein (Figure 4c). The result suggests that the □↑ variant has a higher affinity for Cu^{II} than does the wild-type protein (Table 6). The difference is small, and the outcomes of the approach are sensitive to the experimental conditions, particularly to buffer pH. However, the experiments for □↑ and □□ were carried out in tandem with the same reagent solutions. The result is confirmed by the observation of spontaneous transfer of Cu^{II} from wild-type □Cu^{II} to □↑ (see below). While Glu27 is not a ligand of Cu^{II} in either the high or low pH crystals of the Cu^ICu^{II} form of □□ reported here (Figure 7), its carboxylate oxygen atom is involved in a tight hydrogen bond (2.8 Å) with the N-terminal nitrogen atom of the *apo*-H91F protein □↓ (Figure 8). The equivalent distance is much longer (4.2 Å) to the N-terminal ligand of the high pH Cu^ICu^{II} form of □□. Complete loss of this hydrogen bonding

(50) A previous approach employed sequential titration techniques and provided an estimate of $K_D(\square Cu^{II}) = 10^{-15}$ M.[24] In the present work, equilibrium 2 was approached from both directions, avoiding equilibration errors inherent in the sequential titration technique and allowing the more reliable estimate of $K_D(\square Cu^{II}) = 10^{-13}$ M.

(51) Deschamps, P.; Kulkarni, P. P.; Gautam-Basak, M.; Sarkar, B. *Coord. Chem. Rev.* **2005**, *249*, 895−909.

Table 6. Estimation of Dissociation Constant $K_D(\square Cu^{II})$ for Cu^{II} Bound to CopC by Competition with Ligand egta in 20 mM KPi (pH 7.0), 0.1 M NaCl[a]

protein	$[Cu^{II}]_{tot}$ (μM)	$\Delta F_X/\Delta F_1$[b]	$[Cu^{II}P]$ (μM)	$[Cu^{II}L]$ (μM)	$\{[P]_{tot}/[CuP]\} - 1$	$\{[L]_{tot}/[CuL]\} - 1$	K_D[c] ($\times 10^{-14}$ M)
Wt $\square\square$[d]	2.5	0.15	0.77	1.73	5.5	1.89	7.3
	3.0	0.19	0.97	2.03	4.2	1.46	7.1
	3.5	0.24	1.22	2.28	3.1	1.19	6.6
	4.5	0.34	1.69	2.81	2.0	0.78	6.3
	6.0	0.47	2.33	3.67	1.1	0.36	8.0
	7.5	0.65	3.25	4.25	0.5	0.18	7.7
E27G $\square\uparrow$	2.5	0.23	1.13	1.38	3.4	2.64	3.3
	3.0	0.27	1.34	1.66	2.7	2.02	3.4
	3.5	0.31	1.56	1.94	2.2	1.58	3.5
	4.5	0.42	2.11	2.39	1.4	1.09	3.2
	6.0	0.58	2.89	3.11	0.7	0.61	3.0
	7.5	0.75	3.75	3.75	0.3	0.33	2.5

[a] $[apo\text{-CopC}]_{total} = [egta]_{total} = 5.0$ μM in each solution. [b] See Materials and Methods for details. [c] At pH 7.0 and 0.1 M ionic strength, $K_A(Cu^{II}\text{-egta}) = 4.0 \times 10^{13}$ M^{-1}.[29] [d] Wild type.

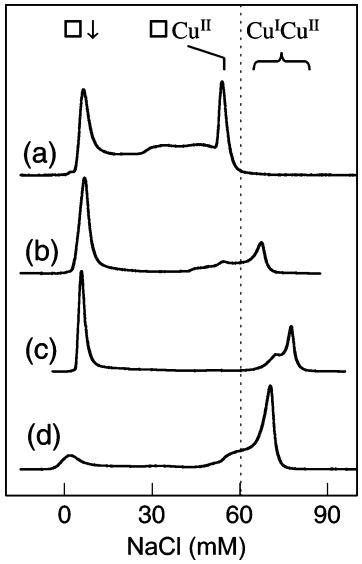

Figure 14. Elution profiles of product H91F CopC proteins on a Mono-S HR5/5 cation exchange column under the conditions of Figure 13. (a) H91F $\square Cu^{II}$ (the increased absorption after elution of $\square\downarrow$ and until elution of H91F $\square Cu^{II}$ is due to progressive production of $\square\downarrow$ from $\square Cu^{II}$ via competition for Cu^{2+} between $\square\downarrow$ and the Mono-S resin); (b) After oxidation of $Cu^{I}\downarrow$ in air for 2 h (the low proportion of product $Cu^{I}Cu^{II}$ and the complex behavior observed in the [NaCl] range 45−60 mM is due to the two step nature of reaction 12 and progressive production of $\square\downarrow$ and $\square Cu^{II}$ via competition for Cu^{2+} between $Cu^{I}Cu^{II}$ and the Mono-S resin (cf. Figures 13b, 14a)); (c) After reduction of H91F $\square Cu^{II}$ by NH_2OH for 2 h. (d) H91F $Cu^{I}Cu^{II}$.

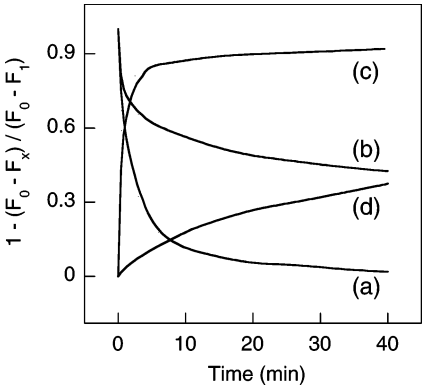

Figure 15. Change in fluorescence emission intensity as expressed as Cu^{II} site vacancy $\{1 - (F_0 - F_x)/(F_0 - F_1)\}$ at 320 nm of CopC proteins (5.0 μM) in KPi (20 mM; pH 7). Introduction of (a) air into wild-type $Cu^{I}\square$ solution (eq 9); (b) air into H91F $Cu^{I}\downarrow$ solution (Figure 14b). About half of the fluorescent intensity is quenched; (c) ascorbate (150 μM) into H91F $\square Cu^{II}$ (50 μM) solution (eq 13; for wild-type protein $\square Cu^{II}$, a full increase in intensity also occurred but over a time scale of 1.5 h (a drop in intensity due to ascorbate absorption at $\lambda_{ex} = 290$ nm was corrected using apo-CopC as a control under the same conditions); (d) NH_2OH (50 μM) into H91F $\square Cu^{II}$ solution (Figure 14c; for wild-type protein $\square Cu^{II}$, the increase in intensity was < 10% that of (c)).

interaction in the E27G variant protein $\square\uparrow$ should increase the basicity of the N-terminal amine and hence its ligand strength. Plausibly, this is the origin of the increased affinity of $\square\uparrow$ for Cu^{2+}.

The derived order of magnitudes of $K_D(\square Cu^{II})$ for the wild-type and variant proteins is summarized in eq 8:

$$\square X > 10^{-5} > \square\downarrow > \square\square = 10^{-13(1)} > \square\uparrow \qquad (8)$$

The high affinity of wild-type CopC for both Cu^{I} and Cu^{II} is consistent with a role as a copper scavenging protein in the oxygenated periplasm. The aerobic stability of the doubly loaded $Cu^{I}Cu^{II}$ form may allow CopC to transport both Cu^{I} and Cu^{II} in that environment.

Intermolecular Copper Transfer with Change of Oxidation State. From the Cu^{I} Site to the Cu^{II} Site. The Cu^{I} form of wild-type CopC ($Cu^{I}\square$) has an empty Cu^{II} site and was air-sensitive. Exposure of a solution of $Cu^{I}\square$ to air caused the fluorescence intensity to drop rapidly ($t_{1/2} < 6$ min) to a level indistinguishable from that of $\square Cu^{II}$ under the same conditions (Figure 15a; cf. Figure 4a,b1). Clean recovery of $\square Cu^{II}$ (yield > 90%) was effected by cation exchange chromatography (cf. Figure 13c). $Cu^{I}\square$ had been oxidized and converted to $\square Cu^{II}$ (O_2^- is assumed to be the initial reduction product):

$$Cu^{I}\square + O_2 \rightarrow \square Cu^{II} + O_2^- \qquad (9)$$

This reaction appears to be driven by oxygen reduction in the presence of an empty high affinity site for Cu^{II}. Consequently, when the Cu^{II} site was occupied ($Cu^{I}Cu^{II}$) or disabled by mutation ($Cu^{I}X$), the bound Cu^{I} was stable. In fact, these latter forms could be chromatographed in air (Figure 13b,e; Table 2, entries 2,5). However, they became air-sensitive in the presence of *apo*-CopC ($\square\square$; Figure 13c,f; Table 2, entries 3,4):

$$Cu^{I}Cu^{II} + \square\square + O_2 \rightarrow 2\,\square Cu^{II} + O_2^- \qquad (10)$$

$$Cu^{I}X + \square\square + O_2 \rightarrow \square Cu^{II} + \square X + O_2^- \qquad (11)$$

These are intermolecular oxidative copper transfer reactions. Reaction 10 provides a model for the oxidation of $Cu^{I}\square$ by O_2 to $\square Cu^{II}$ and suggests that both $\square\square$ and $Cu^{I}Cu^{II}$ may be intermediates in reaction 9:

$$2\ Cu^{I}\square \xrightarrow{O_2} Cu^{I}Cu^{II} + \square\square \xrightarrow{O_2} 2\ \square Cu^{II} \qquad (12)$$

Indeed, for reaction 9 involving the H91F variant $Cu^{I}\downarrow$ (with significantly lower Cu^{II} affinity: eq 8), both species $Cu^{I}Cu^{II}$ and $\square\downarrow$ were isolable (Figures 14b, 15b; Table 2, entries 6,8, footnote f). In this case, the second step of reaction 12 does not go to completion due to lower affinity for Cu^{II}.

From the Cu^{II} Site to the Cu^{I} Site. Under anaerobic conditions, the wild-type protein $\square Cu^{II}$ reacted with ascorbate (asc) with full recovery of fluorescence intensity (Figure 15c), consistent with eq 13:

$$\square Cu^{II} + asc \rightarrow Cu^{I}\square + asc^{+} \qquad (13)$$

While $\square Cu^{II}$ reacted slowly and incompletely with the weaker reductant NH_2OH under the same conditions, the affinity of the H1F variant ($\square$X) for Cu^{II} is so low that even NH_2OH converted the H1F protein $\square Cu^{II}$ to air-stable $Cu^{I}X$ readily and quantitatively (Figure 13e; Table 2, entry 5). Reaction 13 would seem to be driven by ascorbate oxidation in the presence of a high affinity site for Cu^{I}. It is complementary to eq 9 above, but now the transfer is from the Cu^{II} site to the Cu^{I} site. This view is substantiated by the observation that wild-type $Cu^{I}\square$ is air-sensitive while $Cu^{I}X$ is air-stable. The latter can be isolated chromatographically in air, a property shared with the wild-type $Cu^{I}Cu^{II}$ form (Figures 13b,e; Table 2, entries 2,5).

In the case of the H91F variant $\square\downarrow$, incubation of its half-loaded Cu^{II} form $\square Cu^{II}$ with NH_2OH (10 equiv) under anaerobic conditions increased the fluorescence intensity by about one-half of that induced by reduction of $\square Cu^{II}$ with asc under the same conditions (Figure 15c,d). Chromatography of the NH_2-OH solution on the Mono-S cation exchange column showed the recovered H91F protein to be present essentially in its *apo* and $Cu^{I}Cu^{II}$ forms (Figure 14c; Table 2, entries 6,8). As the former protein exhibits its full fluorescence intensity while the latter is fully quenched, the observations are consistent with the following reaction:

$$\text{H91F:}\ \ 2\ \square Cu^{II} + NH_2OH \rightarrow \square\downarrow + Cu^{I}Cu^{II} \qquad (14)$$

Reaction 14 is equivalent to the reverse of reaction 10 for the wild-type protein. It may act as a model for reaction 13 (cf. eq 12):

$$2\ \square Cu^{II} \xrightarrow{asc} Cu^{I}Cu^{II} + \square\square \xrightarrow{asc} 2\ Cu^{I}\square \qquad (15)$$

Taken together, the above experiments demonstrate clearly that the $Cu^{I}\square$ and $\square Cu^{II}$ forms can be exchanged cleanly by oxidation and reduction with effective migration of the copper atom between the two separated high affinity binding sites via intermolecular copper transfer. The oxidation and reduction reactions are coupled to the copper binding affinities.

Intermolecular Copper Transfer without Change of Oxidation State. Cu^{I} Transfer. Differences in copper binding affinity or occupancy will create a thermodynamic gradient for copper transfer without change in oxidation state, provided that the kinetic barrier is low. Indeed, incubation of the H1F protein

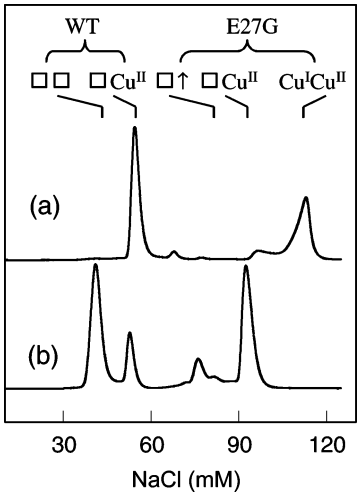

Figure 16. Elution profiles of product CopC proteins under the conditions of Figure 13. (a) Reaction of *either* wild-type $Cu^{I}Cu^{II}$ and E27G $\square Cu^{II}$ *or* wild-type $\square Cu^{II}$ and E27G $Cu^{I}Cu^{II}$ (cf. eq 17); (b) reaction of *either* wild-type $\square Cu^{II}$ and E27G $\square\uparrow$ *or* wild-type $\square\square$ and E27G $\square Cu^{II}$ (cf. eq 18).

$Cu^{I}X$ with wild-type $\square Cu^{II}$ induced clean transfer of Cu^{I} (Figure 13g; Table 2, entries 2, 4):

$$Cu^{I}X + \square Cu^{II} \rightarrow \square X + Cu^{I}Cu^{II} \qquad (16)$$

Intermolecular transfer of copper has occurred but now without a change in oxidation state (cf. eqs 9, 13). The air sensitivity of $Cu^{I}\square$ and the requirement to identify the reaction products after separation on the Mono-S cation exchange column mean that it is difficult to cleanly effect the equivalent reaction between the wild-type half-loaded forms (competing reactions 9 and 10 are rapid on the chromatographic time scale). However, the quantitative transfer of Cu^{I} from $Cu^{I}X$ to wild-type $\square Cu^{II}$ demonstrated that the latter protein has a higher affinity for Cu^{I} than does the variant $\square$X. This might originate in two ways: (i) occupation of the Cu^{II} site in wild type $\square\square$ increases the affinity for Cu^{I} at the Cu^{I} site ($\sim$30 Å away); (ii) mutation at the Cu^{II} site in the variant $\square$X decreases the affinity for Cu^{I} at the Cu^{I} site of $\square$X. The following observations favor the first suggestion. First, the *apo* ($\square\downarrow$) and $Cu^{I}Cu^{II}$ forms of the H91F variant are isolable intermediates in the course of oxidation of its $Cu^{I}\downarrow$ form (Figure 14b; Table 2, entries 6,8) or reduction of its $\square Cu^{II}$ form (Figure 14c; Table 2, entries 6,9). This behavior is consistent with both copper centers in H91F $Cu^{I}Cu^{II}$ being more stable than those in the respective half-loaded forms $Cu^{I}\downarrow$ and $\square Cu^{II}$. Indeed, the H91F $Cu^{I}Cu^{II}$ protein was more stable on Mono-S resin than the $\square Cu^{II}$ form (Figure 14a,d). Second, the Hg^{II} binding affinity at the Cu^{I} site of the wild-type protein is higher when the Cu^{II} site is occupied by Cu^{II} rather than by Hg^{II} (cf. eq 5; Figure 11b,c). Third, incubation of wild-type Cu^{I}-Cu^{II} with E27G $\square Cu^{II}$ also induced a clean Cu^{I} transfer reaction (Figure 16a; Table 2, entries 3,12):

$$\underset{\text{(wild type)}}{Cu^{I}Cu^{II}} + \underset{\text{(E27G)}}{\square Cu^{II}} \rightarrow \underset{\text{(wild type)}}{\square Cu^{II}} + \underset{\text{(E27G)}}{Cu^{I}Cu^{II}} \qquad (17)$$

There is a mutation close to the Cu^{II} site in E27G, but reaction 17 favors the opposite direction from that of reaction 16. It has been demonstrated that mutation of Glu27 to Gly enhances Cu^{II} affinity relative to wild type (cf. eq 8; Figure 4). Consequently,

a decrease or increase in the affinity for Cu^{II} has led to a commensurate decrease or increase in affinity for Cu^{I} at sites separated by 30 Å. The structural basis for such subtle effects is not yet apparent. However, a variation in $K_D(Cu^{I}\square)$ of 1 or 2 orders of magnitude only is necessary to induce the shifts in equilibrium apparent in reactions 16 and 17. This corresponds to a free energy change of less than 3 kJ mol^{-1} only.

Significantly, reactions 16 and 17 were carried out under aerobic conditions in the absence of reductants. The transferring Cu^{I} ions were protected against oxidation by O_2. When reaction 16 was carried out under anaerobic conditions, there was a marginal increase only (~5%) in the yield of $Cu^{I}Cu^{II}$ protein isolated from the Mono-S column with a concordant decrease in the level of detected $\square Cu^{II}$. Such minor differences are at the detection limits. In addition, the sulfonate groups of the Mono-S resin exhibit a high affinity for Cu^{2+} ions and promote slow oxidation by air of both $Cu^{I}Cu^{II}$ (Figure 13b) and $Cu^{I}X$ (Figure 13e). Consequently, direct intermolecular contact must be involved in the Cu^{I} transfer of reactions 16 and 17. The viability and flexibility of such direct "head-to-head" intermolecular contact have been demonstrated from the X-ray crystal structures of $Cu^{I}Cu^{II}$-CopC described above. The contact modes vary at high pH and low pH with the multiple Met residues at the Cu^{I} site switching between Cu^{I}-bridge binding and hydrophobic interactions. Multiple hydrogen bonding interactions may also contribute importantly to such direct intermolecular contact. These experiments confirm that CopC has the potential to transfer Cu^{I} to its partners in the periplasm in the presence of air.

Cu^{II} Transfer. Transfer of bound Cu^{II} between CopC molecules is demonstrated in Figure 16b; Table 2, entries 1,13:

Favors right-hand side (> 70%):

$$\underset{\text{(E27G)}}{\square^{\uparrow}} + \underset{\text{(wild type)}}{\square Cu^{II}} \leftrightarrow \underset{\text{(E27G)}}{\square Cu^{II}} + \underset{\text{(wild type)}}{\square\square} \quad (18)$$

Reaction 18 is a Cu^{II} version of reaction 17. The forward reaction does not go to completion, but the E27G protein binds Cu^{2+} more strongly than does the wild-type protein (eq 8; Figure 4c). E27 is not a Cu^{II} ligand but may compete with Cu^{2+} for the amino terminus (see discussion above on origin of difference in $K_D(\square Cu^{II})$ for the wild-type and E27G proteins).

Nature of the Copper Sites in the CopC Protein. This protein appears to be structurally labile as all four copper sites observed in the two crystal forms of $Cu^{I}Cu^{II}$-CopC differ in stereochemistry and/or ligand content. One copper site only features ligands from a single CopC molecule (Figure 7b) while the other three bridge two separate protein molecules (Figures 6, 7a).

The original solution NMR and EXAFS data were consistent with the presence of a mononuclear $Cu^{I}(N-His)(S-Met)_{2\text{ or }3}$ center similar to the trigonal planar $Cu^{I}(N-His)(S-Met)_2$ site characterized recently in the CusF protein.[13,14,20] His 48 was proposed as one ligand with at least two of the four Met residues M40, M43, M46, and M51 completing the coordination sphere (Figure 2). Both His 48 and Met 40 are copper ligands in the high pH crystal form (Figure 6b). The low coordination number and stereochemistry indicate that this is a Cu^{I} site. The water molecule or hydroxo ion W1 lying on the crystallographic two-fold axis is a third potential (bridging) ligand, but the $Cu^{I}-O$ separation of 2.47(8) Å is longer than the range 2.20−2.24 Å observed in relevant synthetic Cu^{I} complexes.[44,46,47] It is probable that the overall structure observed here is a balance between the forces which define the molecular interface (six hydrogen bonds and multiple hydrophobic attractions: see Supporting Information) and the bonding requirements of a structurally labile Cu^{I} site. One or more of the Met residues at 43, 46, and 51 may be ligands in the monomeric protein but contribute to the hydrophobic interactions of the molecular interface in the high pH crystal form. Water W1 may help to stabilize the Cu^{I}(N−His 48)(S−Met 40) centers via ion−dipole interactions (or ion−ion interactions if W1 is deprotonated), interactions which would also stabilize the molecular interface. As these adjacent sites have an identical and high affinity for Cu^{I} ($10^{-7} \geq K_D \geq 10^{-13}$ M for the monomer in solution), it is the structural flexibility of CopC in the region of the sites that determines the nature of the interface. In fact, this interface may be considered as a partial model for the intermolecular exchange of Cu^{I} in solution (reactions 16, 17): the molecular interface between the exchanging molecules is in place (including Met residues which were formally Cu^{I} ligands), but the receiving Cu^{I} site is blocked.

Crystallization at pH 4.6 (low pH crystal form) provided a significantly different structure in this region of the molecule (Figure 6a). There are two adjacent tetrahedral $[Cu(S-Met)_4]^{+}$ centers. The soft ligands and the stereochemistry are consistent with the presence of Cu^{I}. $[Cu^{I}(S-Met)_4]^{+}$ sites have not been observed previously in protein crystal structures but may be relevant for the Met-rich regions in Cu^{I} pumps such as Ctr1 (see ref 28). The loss of ligand His 48 at pH 4.6 may be related to the acidic conditions as the side chain of His 48 (pK_a ~6) may no longer be able to sustain a bonding interaction with Cu^{I}. In fact, it has been recruited to be a Cu^{II} ligand (see discussion below).

The tetragonal stereochemistry of the other two sites suggests the presence of Cu^{II} (Figure 7). The chemistry observed in solution for the Cu^{II} site is consistent with the structure of the mononuclear tetragonal $Cu^{II}N_3O$ center resolved in the high pH crystal form (Figure 7b). The three nitrogen ligand atoms are supplied by the side chains of His 1 and 91 and by the amino terminus. The aqua ligand completes the coordination sphere and is hydrogen bonded to Asp 89. The protonation states of the amine and aqua ligands are not known. For the low pH crystal form, the acidic crystallization conditions (pH ~4.6) appear to have tipped the balance in favor of protonation of the amino terminus (pK_a ~8) rather than formation of a $Cu^{II}-NH_x$ bond (compare Figure 7a and 7b). While the side chains of His 1 and 91 and a water molecule remain as ligands, His A**48 of neighboring molecule A** has been recruited to maintain the tetragonal stereochemistry of Cu^{II} (Figure 7a).

This center is evocative as it provides a model for the intermolecular transfer of copper during the oxidation of $Cu^{I}\square$ by O_2 (reaction 9) or the reduction of $\square Cu^{II}$ by asc (reaction 13). For the oxidative case (reaction 9), the Cu^{II} product ion has been "caught in the act" of intermolecular transfer: His A**48 (previously a Cu^{I} ligand) is transferring the Cu^{2+} ion from the originating Cu^{I} site while ligands His A1 and His A91 from the destination Cu^{II} site have "trapped" the Cu^{2+} ion. Loss of ligand His A**48 and binding of the N-terminal amine ligand are all that is required to complete assembly of the mononuclear Cu^{II} site observed in the high pH crystal form (Figure 7b).

This is the first protein crystal structure which reveals the nature of a coordinate bond between a metal ion and an amino terminus. The ATCUN motif is a Cu^{II}- and Ni^{II}-binding site found at the amino terminus of naturally occurring proteins such as the serum albumins of several species, histatin-5 (a human salivary protein) and the neuropeptide neuromedin-C.[52] It is defined by an available amino terminus, a histidine residue in the third position, and two intervening peptide nitrogens.[53] Although Cu^{II} and Ni^{II} binding has been established for proteins containing this motif, no crystal structures of the metal-bound proteins have appeared to date.

Summary. The CopC protein features two distinct but interdependent binding sites with high and specific affinity for Cu^{I} and Cu^{II}, respectively. When both sites are occupied, Cu^{I}-Cu^{II}-CopC is stable in air. The availability of an unoccupied site of higher affinity induces intermolecular transfer of *either* Cu^{I} or Cu^{II} in the presence of O_2 while buffering concentrations of cupric ion at sub-picomolar levels. This unique copper chemistry is consistent with a role for CopC as a copper carrier in the oxidizing periplasm (Scheme 1). The inherent flexibility of the two Cu-binding loops may provide the structural lability to allow transfer of copper to and/or from multiple partners, with or without a change of oxidation state. The model of Scheme 1 includes the possibility of CopC interacting directly with the soluble multi-copper oxidase CopA, the membrane pumps CopB and CopD, and the sensor protein CopS.

Acknowledgment. A.G.W. thanks the Australian Research Council for support under Grant A29930204. The pAT2 plasmid was a kind gift from Dr. A. R. Thompsett (CERM, University of Florence). M.J.M. was supported by a University of Sydney SESQUI Postdoctoral Fellowship. Ms Mihwa Lee (University of Sydney) is thanked for collecting the X-ray diffraction data for the H91F variant protein. Assoc. Prof. G. J. Howlett (University of Melbourne) is thanked for the sedimentation equilibrium measurements. Mr. Simon James is thanked for Figure 12. Access to the facilities of the Stanford Synchrotron Radiation Laboratory (SSRL) was supported by a travel grant from the Access to Major Research Facilities Program administered by the Australia Nuclear Science and Technology Organization. The SSRL Structural Molecular Biology Program in the USA is supported by the Department of Energy, Office of Biological and Environmental Research, and the National Institutes of Health, National Center for Research Resources, Biomedical Technology Program, and the National Institute of General Medical Sciences.

Supporting Information Available: The PDB codes for the three CopC structures are 2C9P (low pH), 2C9Q (high pH), and 2C9R (*apo*-H91F). Protein characterization data (SDS-PAGE; ESI-MS; $K_D(Cu^{I})$, gel filtration chromatography; Tables S1, S2; Figures S1−S3); derivation of eq 3; X-ray crystallographic information (Figures S4−S6), including a full discussion of the X-ray crystal structures; metal titration data (Figure S7). This material is available free of charge via the Internet at http//pubs.acs.org.

JA058528X

(52) Sankararamakrishnan, R.; Verma, S.; Kumar, S. *Proteins: Struct., Funct., Bioinf.* **2004**, *58*, 211−221.
(53) Harford, C.; Sarkar, B. *Acc. Chem. Res.* **1997**, *30*, 123−130.
(54) Laskowski, R. A.; MacArthur, M. W.; Moss, D. S.; Thornton, J. M. *J. Appl. Crystallogr.* **1993**, *26*, 283−291.

(55) Abbreviations: asc, ascorbate; Asp or E, aspartic acid; bcs, bathocupröine disulfonate; CM, carboxymethyl; Cys or C, cysteine; DE, diethylaminoethyl cellulose; dt, dithionite; edta, *N,N,N′,N′*-ethylenediamine tetraacetic acid; egta, ethyleneglycol-O,O′-bis(2-aminoethyl)- *N,N,N′,N′*-tetraacetic acid; ESI-MS, electrospray ionization mass spectrometry; His or H, histidine; IPTG, isopropyl-*β*-D-thiogalactopyranoside; *I*, ionic strength; KPi, potassium phosphate buffer; mes, 2-(*N*-morpholino)ethanesulfonic acid; Met or M, methionine; NaAc, sodium acetate; NCS, noncrystallographic symmetry; OD, optical density; Phe or F, phenylalanine; SAD, single wavelength anomalous dispersion phasing; Trp or W, tryptophan; wt, wild type; □□, wild-type *apo*-CopC protein; Cu^{I}□, Cu^{I}-CopC; □Cu^{II}, Cu^{II}-CopC; $Cu^{I}Cu^{II}$, $Cu^{I}Cu^{II}$-CopC; □X, apo-H1F variant protein; Cu^{I}X, Cu^{I}-H1F variant protein; □↓, *apo*-H91F variant protein; □↑, *apo*-E27G variant protein.